GeoScienceWorld
Lithosphere
Volume 2024, Number 1, Article ID lithosphere_2023_225, 32 pages
https://doi.org/10.2113/2024/lithosphere_2023_225

Lithosphere

Research Article

Paleogene Sedimentary Basin Development in Southern Nevada, USA

Jens-Erik Lundstern,[1] **Theresa M. Schwartz**,[1] **Cameron M. Mercer**,[2] **Joseph P. Colgan**,[1] **Jeremiah B. Workman**,[1] **and Leah E. Morgan**[2]

[1]*U.S. Geological Survey, Geosciences and Environmental Change Science Center, Denver, CO, 80225, USA*
[2]*U.S. Geological Survey, Geology, Geophysics, and Geochemistry Science Center, Denver, CO, 80225, USA*

Correspondence should be addressed to Jens-Erik Lundstern; jlundstern@usgs.gov

Received 4 July 2023; Accepted 16 December 2023; Published 29 March 2024

Academic Editor: Alex Simms

The cause of the transition from Mesozoic and early Cenozoic crustal shortening to later extension in the western United States is debated. In many parts of the extant Sevier hinterland, now the Basin and Range Province, the sedimentary sections that provide the most direct record of that transition remain poorly studied and lack meaningful age control. In this paper, we present field characterization supported by U-Pb detrital zircon and $^{40}Ar/^{39}Ar$ feldspar ages for ten sections across southern Nevada. We describe a newly identified basin, here named the Fallout Hills basin, which preserves >1.0 km of sedimentary deposits as old as middle Eocene, ca. 48 Ma. Deposition occurred during the 20 m.y. (million years) before the 27.60 ± 0.03 Ma Monotony Tuff blanketed much of south-central Nevada, based on 47.6 Ma and younger detrital zircon maximum depositional ages (MDAs) from near the Pintwater and Spotted Ranges. Elsewhere in southern Nevada, prevolcanic Cenozoic strata commonly form thinner (~100 m), isolated exposures that yield detrital zircon MDAs ≤10 m.y. older than (and in some cases essentially the same age as) the ca. 27–28 Ma ignimbrites that cap the sections. A variable but overall upward-fining facies pattern is observed in both the Fallout Hills basin and the thinner sections. These localized patterns imply topographic changes that are unlikely to reflect plate-scale processes and are not consistent with large-magnitude extension. Instead, variable uplift due to magmatism combined with antecedent topographic relief from thrust faulting and subsequent erosion likely provided accommodation for these deposits.

1. Introduction

Supracrustal rocks often provide some of the only records of topographic evolution and magmatic activity in ancient orogenic systems. They are, therefore, valuable for inferring the geometry, timing, and causal factors of tectonism and for constraining topographic change for use in geodynamic models [1, 2]. There is active debate concerning the fundamental transition that occurred in the western United States (Figure 1) from Mesozoic and early Cenozoic crustal shortening to Neogene basin-and-range extension [3, 4], which has implications for the study of crustal dynamics worldwide, including the stability of compressional orogens and the causes of extension. Sedimentary rocks deposited during this transition are sparse and generally not well studied across Nevada, eastern California, and western Utah, where one model has proposed that Cretaceous shortening thickened the crust sufficiently to support an orogenic highland commonly referred to as the *Nevadaplano* [5], while another has suggested that elevated topography was achieved only later due to south-migrating middle Cenozoic volcanism [3, 6]. Detailed constraints on the timing and setting of deposition would be valuable for understanding surface dynamics and the associated driving forces during this time and would assist with testing between sharply differing models that have been proposed for the region's crustal, paleogeographic, and climatic history (cf. References 2, 3, 7–10).

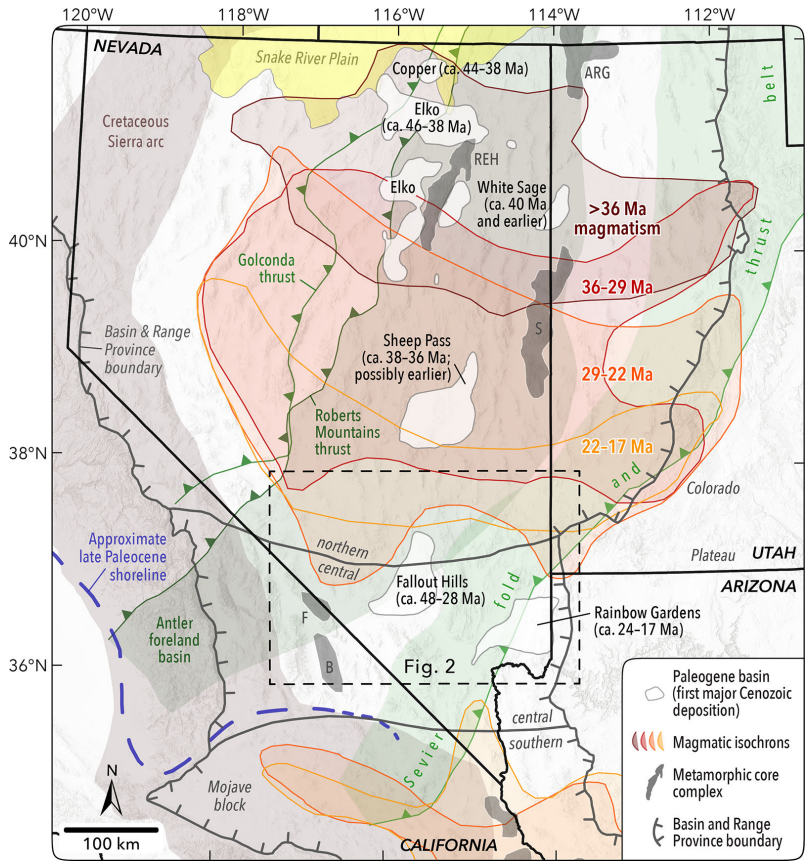

FIGURE 1: Map of geologic features in the northern and central Basin and Range Province, western USA. The Golconda and Roberts Mountains thrusts and Antler foreland basin are from Dickinson [171], and the Sevier fold-and-thrust belt is from DeCelles [5]. The Cretaceous Sierra arc is after Van Buer and Miller [172]. Paleogene basins in the Sevier hinterland are from Haynes [144], Lamb et al. [124], Smith et al. [167], and this study. Their timing of sedimentary deposition is from Dubiel et al. [147], Rahl et al. [14], McGrew et al. [15], Druschke et al. [21], Lund Snee et al. [17], Lamb et al. [124], Canada et al. [11], Lund Snee and Miller [3], and this study. The late Paleocene shoreline is after Reid [173] and Lechler and Niemi [23]. Middle Cenozoic magmatic isochrons are based on ages from this and other studies [3, 38–40, 123, 126, 174] and from NAVDAT (www.navdat.org). Basin and Range Province and subdomain boundaries are modified from Sonder and Jones [175] and Dickinson [176] to more closely follow patterns of physiography, faulting, and gravity anomalies. Metamorphic core complex outlines are after Chapman et al. [177]. ARG, Albion–Raft River–Grouse Creek; B, Black Mountains; F, Funeral Mountains; REH, Ruby–East Humboldt; S, Snake Range.

Cenozoic sedimentary rocks deposited in this region before widespread middle Cenozoic volcanism and Neogene extensional basin fill (Figure 2) are better characterized in parts of northeastern Nevada [3, 11–17], east-central Nevada [18–24], southwestern Utah [25–29], and the Grapevine–Funeral Mountains area of southwestern Nevada and southeastern California [4, 6, 30–35]. Less is known about such deposits in southern Nevada, which are challenging to correlate to one another and to other strata across the region due to poor age control and to having been segmented into different basins by Neogene extensional faulting [27, 36–40].

This paper characterizes sedimentary rocks exposed above the base-Cenozoic unconformity in ten sections in southern Nevada (Figure 2), providing in some cases their first documentation in the published literature. More specifically, our focus is on the mostly middle Cenozoic strata preserved below regionally widespread Oligocene to Miocene volcanic rocks or ca. 17 Ma and younger extensional basin fill (Figure 3). To enable correlation between the prevolcanic strata, we obtained detrital zircon U-Pb ages for sixteen sandstone samples and $^{40}Ar/^{39}Ar$ feldspar ages for six samples of the capping volcanic tuffs. We begin by describing the geologic setting, and then we detail the methods and results of our stratigraphic characterization and geochronology. Based on these results, we outline generalized facies patterns and depositional timing across the studied area. We conclude by discussing implications for understanding the region's paleogeographic and tectonic evolution between Late Cretaceous and late Cenozoic time.

1.1. Geologic Setting. The study area is located in parts of southern Nevada that lie to the north of the Las Vegas Valley shear zone, broadly around 37°N latitude (Figure 2). This area is situated between the southern Sierra Nevada and western Colorado Plateau, and it straddles the boundary between the northern and central subdomains (Figure 1) of the Basin and Range Province. Moving south over this subdomain boundary, there is a marked *decrease* in mean elevations and in the width of the province, as

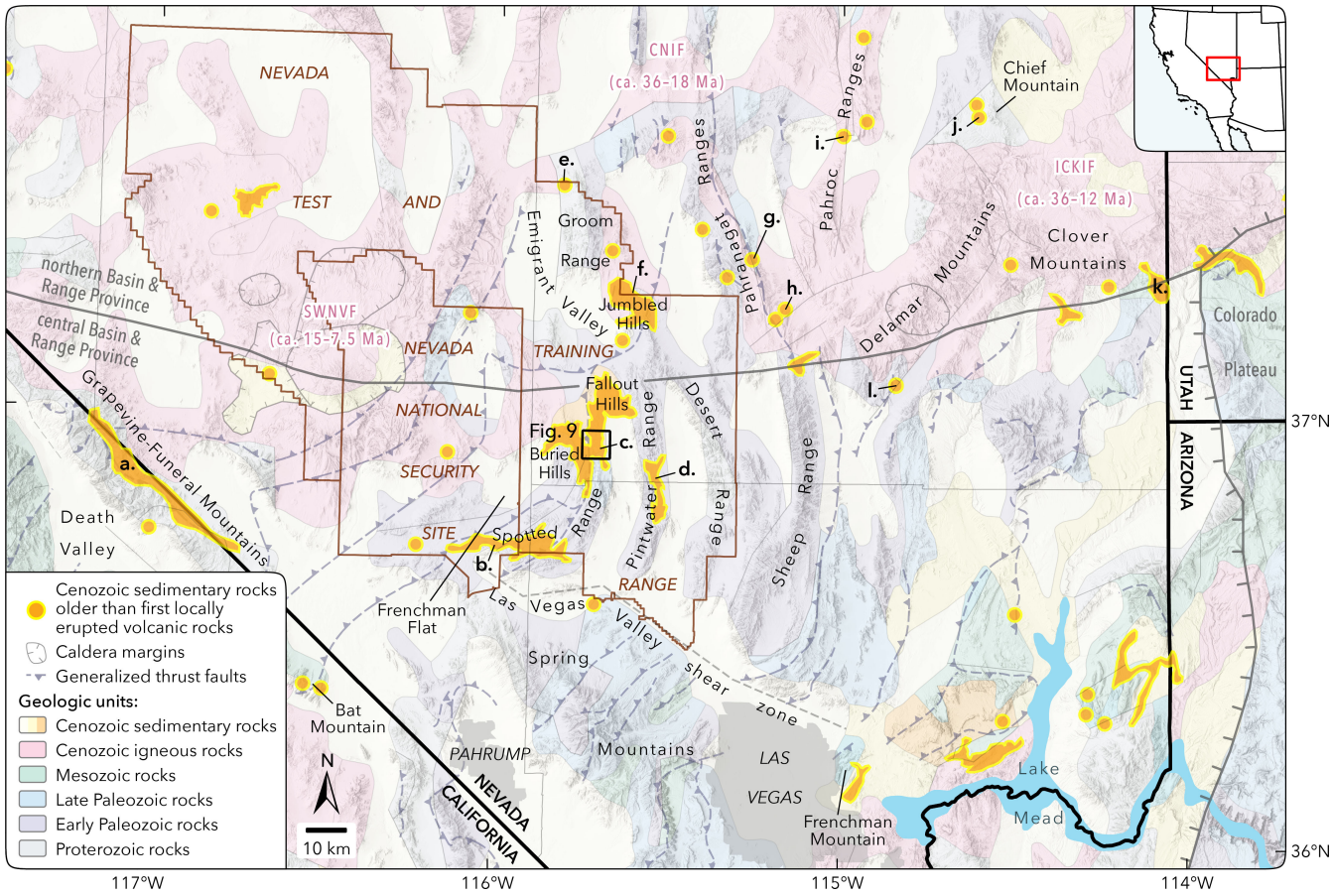

FIGURE 2: Generalized geologic map of southern Nevada after Garrity and Soller (2009). The study area includes areas north of the latitude of Las Vegas. Exposed extents of middle Cenozoic sedimentary rocks that were deposited before the first locally erupted volcanic rocks are greatly simplified from Taylor [27], Workman et al. [38], Jayko [39], Beard et al. [178], Biek et al. [88], Lundstern et al. [79], Schwartz et al. [35], and this study. Basin and Range Province and subdomain boundaries are modified from Sonder and Jones [175] and Dickinson [176]. Thrust faults are generalized from Tschanz and Pampeyan [40], Stewart and Carlson [179], Wernicke et al. [180], Workman et al. [38], Page et al. [181], Rowley et al. [80, 128], Biek et al. [88], Felger and Beard [182], and Lundstern et al. [79]. Ages are from Sawyer et al. [183] for the southwestern Nevada volcanic field (SWNVF); from Best et al. [126] for the central Nevada ignimbrite field (CNIF); and from Rowley et al. [184], Nealy et al. [185], and Best et al. [123] for the Indian Peak–Caliente–Kane Springs Wash ignimbrite fields (ICKIF). Letter labels correspond to stratigraphic columns in Figure 4: a—Grapevine–Funeral Mountains (Titus Canyon); b—Frenchman Flat; c—northeastern Spotted Range and Fallout Hills; d—eastern Pintwater Range; e—northern Groom Range; f—northern Jumbled Hills; g—East Pahranagat Range; h—southeastern East Pahranagat Range (Arrowhead Mine fault section); i—southern North Pahroc Range; j—Chief Mountain; k—Dodge Spring (Clover Mountains); l—southern Delamar Mountains.

well as an *increase* in surface heat flow, Bouguer gravity anomaly, and the prevalence of strike-slip faulting in both the Neogene deformational history and the present-day stress field [41–46]. An active seismic belt situated along the northern part of the transition zone accommodates dominantly left-lateral offset [47], whereas Cenozoic volcanism largely did not occur south of this transition, in a zone between ~36°N and 37°N (Figure 2) that has been termed the magmatic gap [42, 48, 49]. Despite these contrasts, the first rapid extension in both areas occurred in middle Miocene time, ca. 17–15 Ma, resulting in rapid basin-filling sedimentation and eventually culminating in the region's present-day basin-and-range topography [50–60].

Throughout the study area, Cenozoic sedimentary rocks unconformably overlie Neoproterozoic, Paleozoic, and Mesozoic rocks across what we refer to regionally as the base-Cenozoic unconformity (Figure 3). At the base of the pre-Cenozoic succession, the crystalline basement is overlain by Neoproterozoic to Cambrian clastic sedimentary rocks deposited during the rifting of the Rodinia supercontinent [61]. Those strata are covered by a westward-thickening wedge of passive margin carbonate and clastic rocks [62], which is capped by late Paleozoic deposits of the Antler foreland (Figure 1) and successor basins [63–71].

The Neoproterozoic to Paleozoic strata were deformed by Mesozoic thrust faults, which in southern Nevada were usually characterized by thin-skinned ramp–flat geometries. Jurassic thrust faults were concentrated between the present-day Sierra Nevada in southeastern California and south-central Nevada [72–75], whereas Early Cretaceous

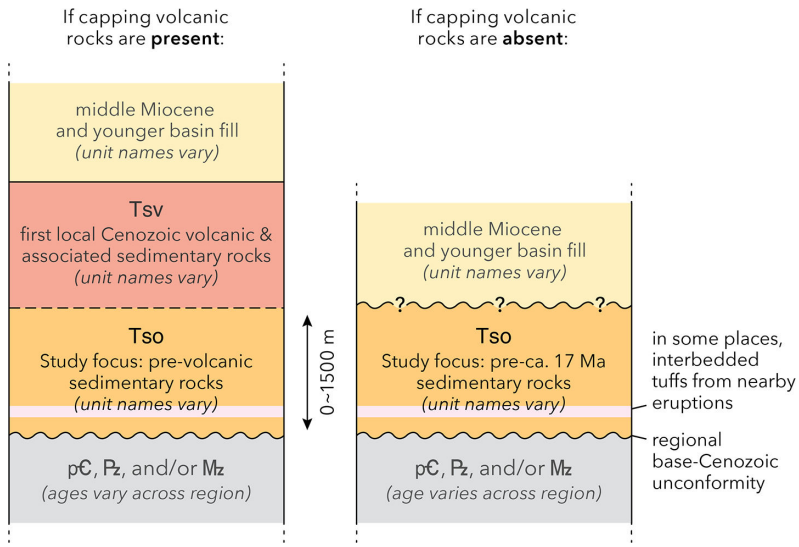

Figure 3: Schematic sections illustrating the prevolcanic Cenozoic sedimentary rocks (in orange and labeled Tso, although unit names vary) that are the focus of this study. The dashed line indicates a possible transitional contact.

to early Eocene thrust faults of the Sevier orogeny are mostly exposed farther east [76–78]. The Sevier fold-and-thrust belt extends southwest from southwestern Utah to cover parts of southern Nevada (Figure 1), with a hinterland that extends into the northwestern part of the study area. Figure 2 shows a generalized view of major thrust faults, of which several are exposed near deposits of the target prevolcanic Cenozoic sedimentary rocks, including in the Delamar Mountains and the Spotted, Pahranagat, and Sheep Ranges. To the north of the Las Vegas Valley shear zone (Figure 2), in the areas of interest for this study, thrust faults typically place the latest Neoproterozoic and lower Paleozoic strata over upper Paleozoic strata and strike roughly north–south or northeast–southwest [38–40, 79–84]. The timing of thrust faulting is not well constrained in the study area, but a Late Jurassic to middle Cretaceous age range has recently been suggested based on zircon (U-Th)/He thermochronology of samples from the Spring Mountains that have been structurally correlated with the Gass Peak thrust in the Sheep Range [74].

Although the Late Cretaceous to Eocene Laramide orogeny partly overlapped in time and space with Sevier shortening in parts of the Cordilleran retroarc, its characteristic thick-skinned deformation occurred east of the Sevier thrust front at the latitudes of southern Nevada [26, 85, 86], outside the study area. Basement-cored Laramide uplifts disrupted the extensive Sevier foreland basin system, and they were accompanied by their own sedimentary basins [87], including the greater Claron Basin of southwestern Utah and easternmost Nevada, which filled with Late Cretaceous to Eocene or Oligocene rocks [25, 27, 28, 88]. The shallowly subducting Farallon slab, which is thought to have caused the Laramide uplifts by interacting with the overlying continental crust (see Reference 89), apparently underlay the study area in southern Nevada beginning in the Campanian (Late Cretaceous) [90]. Starting in the Eocene, near the end of the Laramide orogeny, the Farallon slab is inferred to have progressively fallen away from the base of the continent [91], leading to an episode of intense, caldera-forming volcanism that expanded southward across the western United States into the early Miocene (Figure 1), blanketing some areas in thick (>1 km) ignimbrites and lava flows [48]. Lund Snee and Miller [3] proposed that this magmatism contributed to perhaps 1 km of southward-migrating surface uplift that disrupted existing drainage networks across Nevada between the middle Eocene and early Miocene time.

This study focuses on the Cenozoic sedimentary rocks that are variably preserved above the base-Cenozoic unconformity, occurring below the ca. 17 Ma and later extensional basin fill (Figure 3). Because these oldest Cenozoic rocks usually underlie the volcanic rocks of the ignimbrite flare-up, we collectively refer to them as prevolcanic middle Cenozoic deposits, although we recognize that synchronous volcanism was usually active farther to the north, and at times even in the area of the deposits themselves (e.g., the North Pahroc Range, described below). These middle Cenozoic sedimentary deposits have received little attention and typically form isolated exposures that have been partitioned by Neogene normal and strike-slip faulting (Figure 2). Consequently, most have been challenging to correlate, and many lack formal stratigraphic names (see References 37, 92). Our new reconnaissance characterization and age control enable us to place a number of these sections in regional and temporal contexts.

2. Methods

2.1. Field Methods. We selected sections by identifying the stratigraphically lowest Cenozoic sedimentary rocks (usually those exposed below the first volcanic rocks) from prior geologic mapping (e.g., Reference 38), satellite imagery, and field characterization. Figure 3 is a

schematic illustration of the intervals of interest. Where possible, we sampled their highest, lowest, and sometimes intermediate exposures for detrital zircon U-Pb analysis. We sought indurated, fine- to medium-grained sandstone to limit contamination by younger sediments. To further prevent contamination, we sought material that was not exposed to the surface or root networks, removed visibly adhered material, blew off dust, and rinsed sufficiently indurated samples with tap water before mineral separation. We also sought samples of the lowest exposures of capping volcanic rocks for $^{40}Ar/^{39}Ar$ geochronology. We sought fresh samples and removed visible weathering rinds, as defined by a marked color change in the direction of the exposed surface, and we rinsed samples with tap water before mineral separation.

We measured the stratigraphic section at the Arrowhead Mine fault locality on the southeastern flanks of the East Pahranagat Range (Figures 2 and 4(h)) at 10-cm resolution using a Jacob staff and clinometer. Thicknesses for the other sections were not measured directly in the field, usually because portions of the sections were not exposed due to faulting, erosion, or alluvial cover. Access restrictions on the military land of the Nevada Test and Training Range (NTTR) and former nuclear weapons testing areas of the Nevada National Security Site (NNSS; Figure 2) limited our ability to conduct a detailed characterization of certain sections. We were granted access to the northeastern flanks of the Spotted Range and the eastern flanks of the Pintwater Range within the NTTR (Figures 2 and 4(c)-(d)) during limited hours, whereas scientific research is completely prohibited elsewhere such as in the Fallout Hills.

For most sections, we estimated true stratigraphic thicknesses using trigonometric relationships [93]. Data for these calculations were obtained from satellite imagery (e.g., U.S. Geological Survey/National Aeronautics and Space Administration Landsat, Copernicus/Maxar Technologies, and Center National d'Etudes Spatiales/Airbus), geologic maps [36, 38, 40, 79, 83, 92, 94; this study], and bedding attitudes measured in the field. In some cases, bedding orientations were supplemented by attitudes that we determined from three-point problems using published geologic maps, satellite imagery, and topographic data. Annotated satellite images in online supplementary material Figures S1-S10 show the locations of section thickness estimates and field samples. Thicknesses and internal stratigraphy of the section south of Frenchman Flat (Figures 2 and 4(b)), which we did not visit, are inferred from geologic mapping by Barnes et al. [84]. Data for the Titus Canyon section in the Grapevine–Funeral Mountains (Figures 2 and 4(a)) are from Miller et al. [6].

2.2. $^{40}Ar/^{39}Ar$ Geochronology. Mineral separation for $^{40}Ar/^{39}Ar$ geochronology was conducted at ZirChron, LLC, in Tucson, AZ, using standard techniques. Six igneous samples were disaggregated using a Retsch BB100 jaw crusher and Bico disk pulverizer. Samples were then subjected to density separation using a water table, followed by passes through a vertical Frantz separator, and finally immersion in successively denser concentrations of methylene iodide. A nonmagnetic density fraction between 2.50 and 2.55 g/cm^3 was employed for $^{40}Ar/^{39}Ar$ analysis. Feldspar grains were etched in a 10% HF solution for 20 minutes to remove matrix material.

Detailed analytical methods are provided in an accompanying U.S. Geological Survey Data Release [95]. Briefly, the minerals, together with neutron flux monitor FCs (28.201 ± 0.023 Ma, 1σ) [96], were irradiated at 0.8 MW for 7.5 hours (6 MWh total energy) by fast neutrons in the central thimble of the U.S. Geological Survey TRIGA reactor [97]. J values were calculated using methods outlined by McDougall and Harrison [98] for sixty grains of FCs. These J values formed a unimodal population, so we pooled them to compute an inverse variance-weighted mean value of $1.5469 \times 10^{-3} \pm 1.8 \times 10^{-6}$, which we used to compute apparent ages for all six unknown samples. Mass spectrometry was performed at the U.S. Geological Survey Argon Geochronology Laboratory in Denver, CO. Each sample was degassed using a Photon Machines 50 W CO_2 laser. Purified noble gases were then expanded into a Thermo Scientific ARGUS VI mass spectrometer. Argon isotope data were collected using Pychron v.20.1.1 [99]. Apparent $^{40}Ar/^{39}Ar$ ages were computed using the ^{40}K decay constants of Min et al. [100]: $\lambda_\beta = (4.884 \pm 0.099) \times 10^{-10}$ a^{-1}, $\lambda_{ec} = (0.580 \pm 0.014) \times 10^{-10}$ a^{-1}, and $\lambda_{total} = (5.463 \pm 0.107) \times 10^{-10}$ a^{-1}. We computed standard inverse variance-weighted mean ages (t_{wm}, hereafter referred to simply as weighted mean ages) using $w_i \equiv 1/\sigma_i^2$ and $t_{wm} = \sum_{i=1}^{N} w_i t_i / \sum_{i=1}^{N} w_i$, where t_i and σ_i are the apparent ages and 1σ uncertainties of the analyses, respectively [101]. We assessed the goodness of fit for weighted means by computing the value of the mean squared weighted deviation (MSWD, also called the reduced χ^2 statistic; [101, 102]), which we considered to be acceptable if the MSWD fell below the upper limit of the 95% CI of the MSWD [103]. Where the MSWD exceeded this limit, we performed outlier detection by applying the Hampel identifier [104] to the values $\chi_i^2 = \frac{w_i(t_i - t_{wm})^2}{\sigma_i}$. We identified potential outliers using a permissive cutoff of 6; for all samples analyzed here, the MSWDs became acceptable without progressing to more aggressive (lower) cutoffs.

Figure 5 and online supplementary Table S1 report individual $^{40}Ar/^{39}Ar$ dates with analytical uncertainties, internal uncertainties (which include analytical + J uncertainties), and external uncertainties (analytical + J + ^{40}K decay constant uncertainties). The 2σ external uncertainty is 1.5 Ma for all $^{40}Ar/^{39}Ar$ preferred ages. The text reports the 2σ internal uncertainties, as is conventional for $^{40}Ar/^{39}Ar$ geochronology. Figure 4 additionally provides the full 2σ external uncertainties in parentheses to ensure comparability with the U-Pb detrital weighted mean ages. For samples that

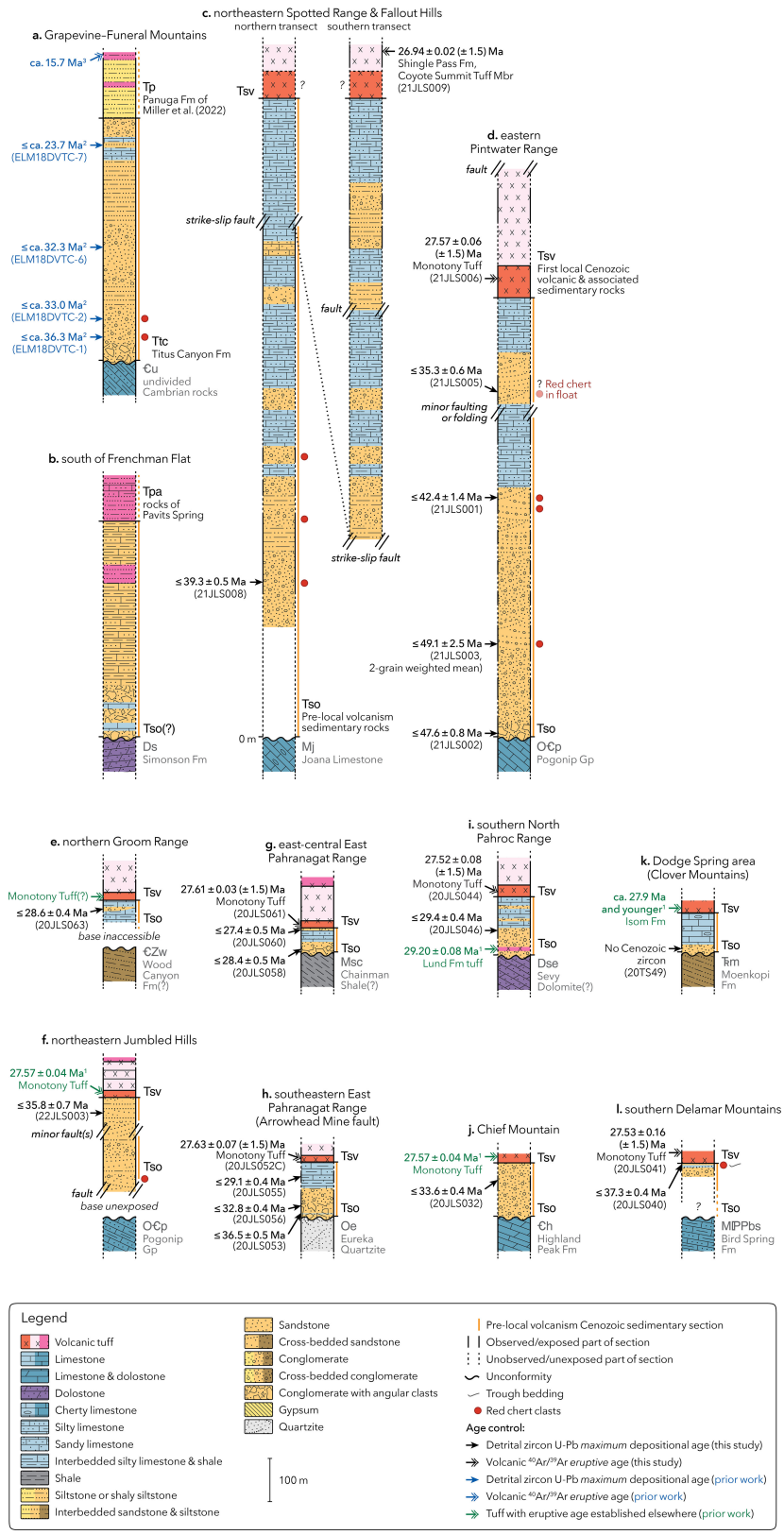

FIGURE 4: Schematic columns for middle Cenozoic stratigraphic sections in southern Nevada and nearby areas. Section locations are shown in Figure 2. 1—Best et al. [48, 49]; 2—Miller et al. [6]; 3—Snow and Lux [31]. Errors for the detrital zircon U-Pb maximum depositional ages from this study (Table 1) are reported at the 2σ level and include both analytical and external uncertainties. Errors for volcanic $^{40}Ar/^{39}Ar$ eruptive ages from this study (online supplementary Table S1) are 2σ internal uncertainties (including uncertainties in *J*). The full external 2σ uncertainties (which also include uncertainty in the ^{40}K decay constant) are reported in parentheses to ensure comparability with the U-Pb ages.

Table 1: Maximum depositional age (MDA) determinations for zircon U-Pb analysis of sedimentary samples.

Sample	Latitude (°WGS84)	Longitude (°WGS84)	Section	Stratigraphic position	MDA (Ma)	MDA uncertainty including external (Ma, 2σ)	Number of grains used for MDA	MDA method
21JLS008	36.9268	−115.7107	Northeastern flanks of Spotted Range	~1/4 up section	39.3	0.54	4	Youngest 3+ ages overlapping within 2σ (YC2σ[3+])
21JLS005	36.8635	−115.5274	Eastern flanks of Pintwater Range	~3/4 up section	35.3	0.61	5	YC2σ(3+)
21JLS001	36.8609	−115.5380	Eastern flanks of Pintwater Range	Middle	42.4	1.37	5	YC2σ(3+)
21JLS003	36.8601	−115.5454	Eastern flanks of Pintwater Range	~1/4 up section	49.1	2.51	*2*	*Youngest 2+ ages overlapping within 1σ (YC1σ[2+])*
21JLS002	36.8609	−115.5496	Eastern flanks of Pintwater Range	Base	47.6	0.80	18	YC2σ(3+)
20JLS063	37.5486	−115.8103	Northern Groom Range	Probably the middle or upper part	28.6	0.25	21	YC2σ(3+)
20JLS060	37.3733	−115.2615	East-central East Pahranagat Range	Top	27.4	0.46	10	YC2σ(3+)
22JLS003	37.2914	−115.6018	Northern Jumbled Hills	Top	35.8	0.66	8	YC2σ(3+)
20JLS058	37.3733	−115.2619	East-central East Pahranagat Range	~1/3 up section	28.4	0.45	10	YC2σ(3+)
20JLS055	37.2581	−115.1633	Arrowhead Mine fault section, southeastern East Pahranagat Range	Near top	29.1	0.37	9	YC2σ(3+)
20JLS056	37.2583	−115.1651	Arrowhead Mine fault section	~1/4 up section	32.8	0.42	25	YC2σ(3+)
20JLS053	37.2594	−115.1655	Arrowhead Mine fault section	Near base	36.5	0.52	4	YC2σ(3+)
20JLS046	37.6609	−114.9976	Southern tip of North Pahroc Range	Probably middle or lower part	29.4	0.39	16	YC2σ(3+)
20JLS040	37.0841	−114.8395	Southern Delamar Mountains	Near top	37.3	0.44	13	YC2σ(3+)
20TS49	37.3025	−114.0553	Dodge Spring, Clover Mountains, NV–UT border	Near base	218.6	4.02	3	YC2σ(3+)
20JLS032	37.7372	−114.6080	Chief Mountain area	~2/3 up section	33.6	0.39	16	YC2σ(3+)

did not consist purely of sanidine, online supplementary Table S1 reports separate weighted mean ages of sanidine grains (identified if K/Ca > 1), nonsanidine grains (K/Ca < 1), and a combination of both phases. For sample 20JLS044, we also filtered data to only include runs with >10% $^{40}Ar^*$ for some weighted mean calculations. online supplementary Table S1 also reports alternative ages if the choice of parameters for outlier detection would significantly affect which grains were included in the weighted mean calculation. For samples that yielded few sanidine grains, we report individual sanidine grain ages for completeness. In general, we prefer weighted mean ages that dominantly include analyses of sanidine or that include one or more grains of sanidine in addition to nonsanidine grains. We acknowledge that the sanidine analyses are usually more precise and can strongly influence the weighted mean ages. However, Table 1 demonstrates that, for the samples analyzed here, the various choices for pooling grains produce indistinguishable age results that do not affect our interpretations.

2.3. Detrital Zircon Geochronology. For nine of sixteen detrital zircon samples, zircon separation for U-Pb analysis was conducted at ZirChron, LLC, using standard techniques. Rock samples were disaggregated using a Retsch BB100 jaw crusher and Bico disk pulverizer. Samples were then subject to density separation employing a Holman-Wilfley 100 water table followed by immersion in methylene iodide (3.3 g/cm^3) and then magnetic separation involving multiple passes through a vertical Frantz separator with a final (highest) power setting of 1.0 A. The denser and less magnetic fraction obtained after these steps was employed for U-Pb analysis.

Zircon was separated from seven additional samples (20JLS040, 20JLS046, 20JLS053, 20JLS055, 20JLS058, 20JLS060, and 20JLS063) at GeoSep Services in Moscow, ID, using standard techniques. Samples were disaggregated, and fine-grained material was extracted using iterative runs through a Chipmunk jaw crusher with maximum jaw separation set to 2–3 mm followed by sieving using 300 μm nylon mesh. The ≤300 μm material that was retained was washed using tap water to remove ultrafine grains and allowed to dry at room temperature. Subsequent density separation employed a centrifuge process with the sample immersed in lithium metatungstate (~2.9 g/cm^3). The denser fraction was then passed through a Frantz magnetic separator, and the less-magnetic fraction was retained. A final step of density separation was conducted using methylene iodide (~3.3 g/cm^3). When necessary, zircon within the dense fraction was further concentrated by hand-panning in acetone.

Zircon separates were mounted in epoxy and then analyzed by laser ablation inductively coupled mass spectrometry (ICP-MS) at the University of Arizona LaserChron Center (supported by National Science Foundation grant NSF-EAR 2050246) following standard techniques [105, 106]. Analysis was conducted on a Thermo Element2 single-collector ICP-MS attached to a Photon Machines Analyte G2 excimer laser. The LaserChron Center supplied standards for age and the isotope fractionation that occurs during the ablation of each laser pit. The primary calibration standard employed for both $^{206}Pb/^{238}U$ and $^{206}Pb/^{207}Pb$ ages was Duluth Complex (FC-1) zircon, which was set to 1100 Ma to correspond approximately with age determinations using the chemical abrasion thermal ionization mass spectrometry (CA-TIMS) and isotope dilution thermal ionization mass spectrometry (ID-TIMS) methods [107, 108]. Sri Lanka (SL-M) zircon served as a secondary reference material for $^{206}Pb/^{238}U$ and $^{206}Pb/^{207}Pb$ ages, with its age set to 564 Ma [106, 109]. Finally, R33 zircon served as a tertiary standard for $^{206}Pb/^{238}U$ ages only, with its age set to 420 Ma [108, 110].

Data were reduced using AgeCalc [106] in combination with AgeCalcML [111]. As is conventional at the LaserChron Center, the $^{207}Pb/^{206}Pb$ age was selected as the preferred age in cases where the mean of the $^{206}Pb/^{238}U$ and $^{207}Pb/^{206}Pb$ ages was ≥900 Ma, and the $^{206}Pb/^{238}U$ age was >400 Ma; otherwise, the $^{206}Pb/^{238}U$ age was selected. Plotting and weighted mean calculations for determining maximum depositional ages (MDAs) employed detritalPy [112]. Analytical data are provided in the Supplementary Material. Age spectra are shown in Figure 6.

We employed the following data reduction parameters and quality filters. Unknown analyses were excluded if $^{206}Pb/^{238}U$ uncertainty was >10%, except for Cenozoic grains, which were excluded if uncertainty was >20%. Analyses were also excluded if $^{207}Pb/^{206}Pb$ age was >700 Ma and $^{207}Pb/^{206}Pb$ uncertainty was >10%. Reference material overdispersion factors were set to default values of 0.6 for $^{206}Pb/^{238}U$ and 1.0 $^{207}Pb/^{235}U$. Individual standard analyses were excluded if their ages were >20% different from the established age. Both unknown and reference material analyses were excluded for discordance between $^{206}Pb/^{238}U$ and $^{207}Pb/^{206}Pb$ ages >20% or reverse discordance >5%. The discordance filter was applied only for $^{206}Pb/^{238}U$ ages >700 Ma. Analyses were excluded if ^{204}Pb was >600 counts s^{-1}, indicating high common Pb. Analyses were also excluded if $^{206}Pb/^{204}Pb$ was <200, except for Cenozoic grains, which were excluded only if $^{206}Pb/^{204}Pb$ was <50 due to the small amount of radiogenic ^{206}Pb relative to the ^{204}Pb baseline in young grains potentially excluding viable analyses. For samples reduced in AgeCalcML, analyses were excluded if they displayed spiky or erratic time series suggesting instrument problems. Finally, analyses were excluded if U concentration was ≥2000 parts per million as a filter for possible radiation damage.

2.4. Calculation and Use of Detrital Zircon U-Pb MDAs. Figure 7 and Table 1 report our new MDAs for sedimentary samples. Of the sixteen detrital samples for which we obtained U-Pb ages (Figure 6), all but one (20TS49) yielded Cenozoic grains. There is inherent subjectivity in the choice of method for estimating MDA and the subset of grains to include in that calculation, of which many competing options have been proposed [35, 113–116]. These choices are made more challenging by the possibility of encountering zircon ages younger than a

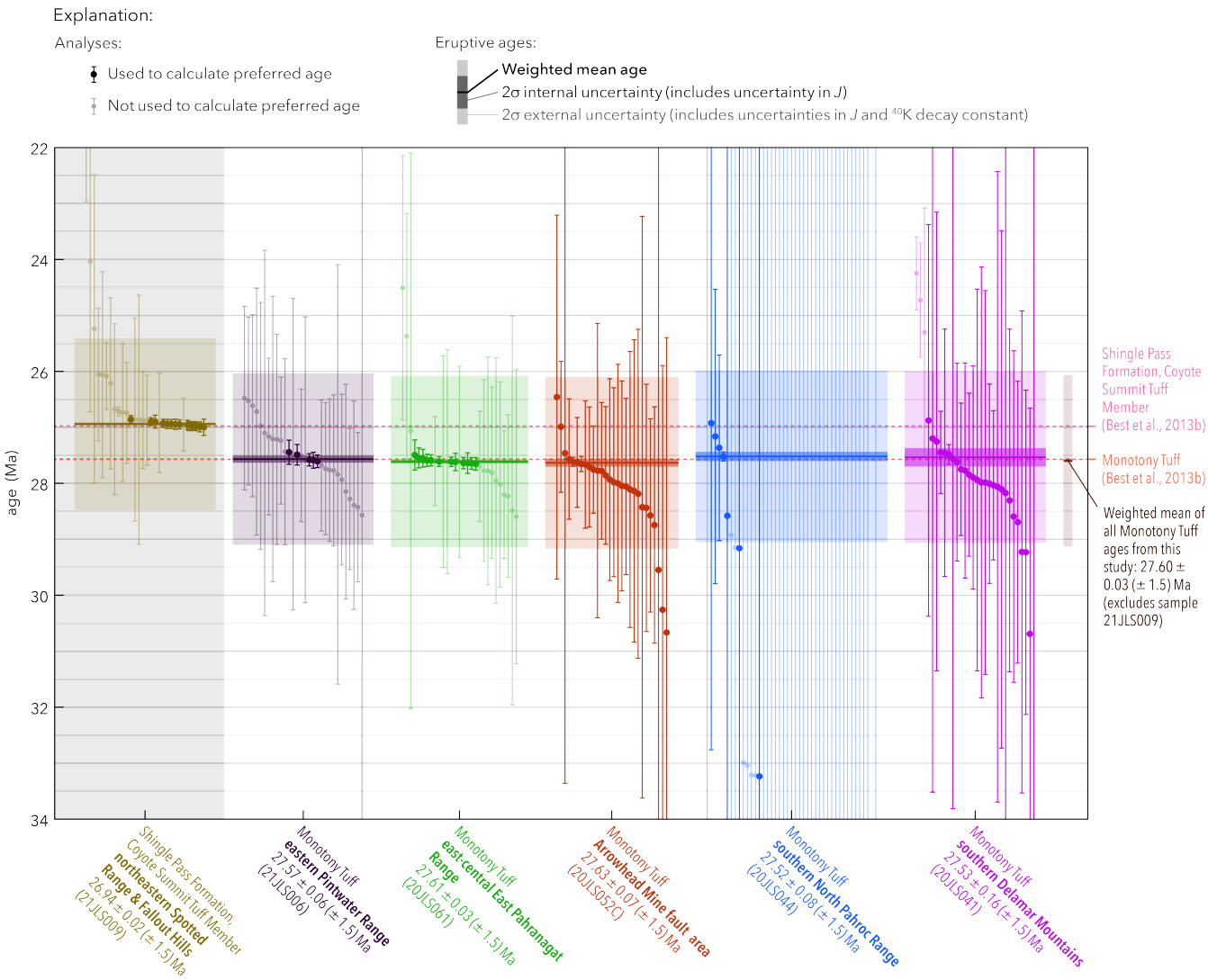

FIGURE 5: Individual grain analysis and weighted mean eruptive ages from $^{40}Ar/^{39}Ar$ feldspar geochronology of volcanic samples. See the text for the filtering criteria for analyses included in the preferred age calculations. Errors for volcanic $^{40}Ar/^{39}Ar$ eruptive ages from this study (online supplementary Table S1) are 2σ internal uncertainties (including uncertainties in *J*). The full external 2σ uncertainties (which also include uncertainty in the ^{40}K decay constant) are reported in parentheses to ensure comparability with the U-Pb ages. Section locations are shown in Figure 2, and sample stratigraphic positions are shown in Figure 4.

sample's true depositional age because of either postcrystallization Pb loss [117–121] or contamination of the sample by younger grains.

We determined MDAs by calculating the weighted mean age of the youngest three or more grains whose ages overlap within 2σ uncertainty (YC2σ[3+]). We employed this widely used method, outlined by Dickinson and Gehrels [113], because the three-grain requirement is relatively conservative while also benefiting from being intuitive, consistent between samples, lacking ambiguity in which a subset of youngest grains to include in the calculation, and easily visualized. For comparison, Figure 7 and the text give the preferred YC2σ(3+) ages, except for the case of the sample (21JLS001) for which only the weighted mean of the youngest two or more ages that overlap within 1σ uncertainty (YC1σ[2+]) could be determined. All uncertainties are reported at the 2σ level. Those in Figure 7 include only analytical uncertainties, whereas those in the text and Table 1 include both analytical and external sources of uncertainty, propagated in quadrature [122].

The detrital zircon MDAs obtained for most of these samples are Cenozoic in age. Although many (but not all) of the strata that we examined lack visible volcanic clasts, nearly all detrital zircon samples yielded middle Cenozoic grains that we interpret to have been derived from ignimbrite flare-up rocks erupted from mostly farther north in the Basin and Range Province, including the Indian Peak–Caliente ignimbrite field [123] to the north and east (Figures 1 and 8). Cenozoic detrital minerals encountered in the prevolcanic sedimentary strata of northern Nevada and southeastern California have been interpreted as wind-blown, originating from distant

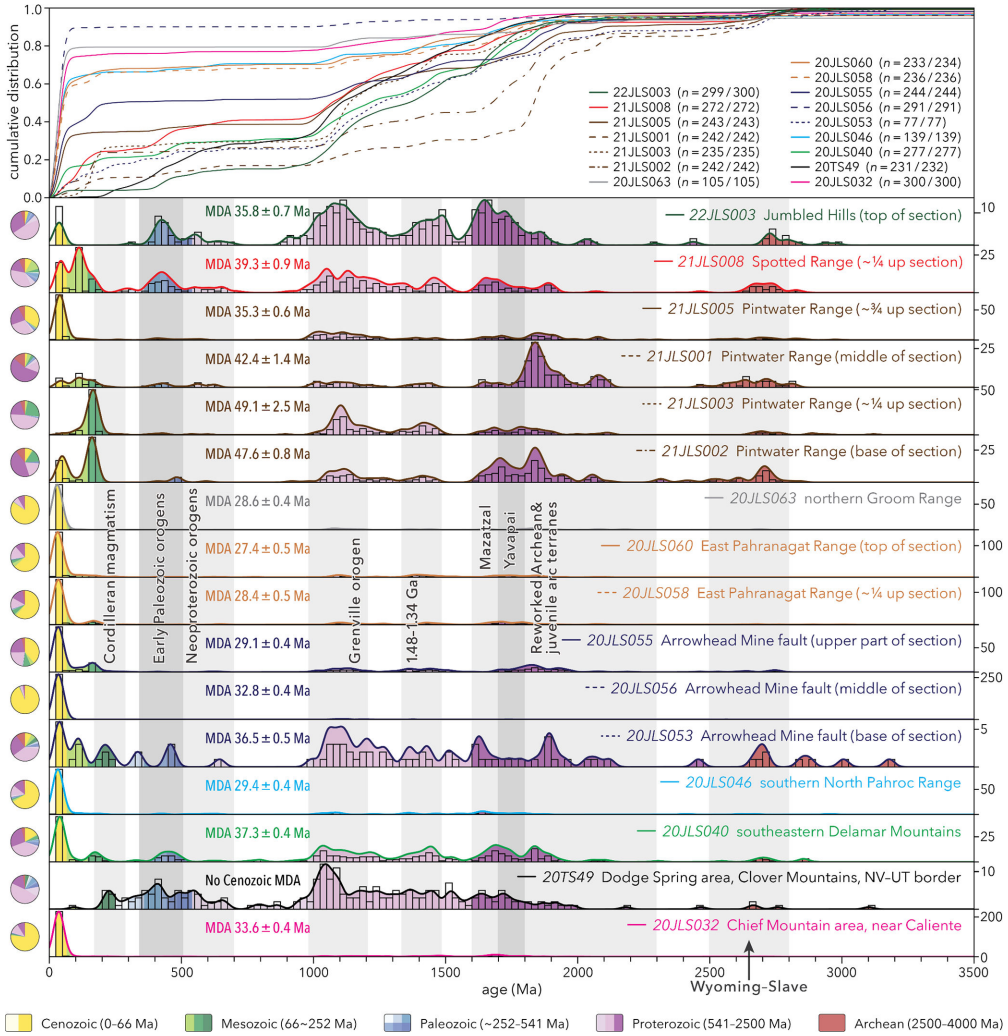

FIGURE 6: Age spectra for detrital zircon U-Pb samples. The top panel shows sample cumulative distribution functions. The other panels are kernel density estimates (KDE) for each sample. KDE bandwidth is 20 m.y., and histogram bin size is 25 m.y. Age on the pie charts increases clockwise from the top. Section locations are shown in Figure 2, sample stratigraphic positions are shown in Figure 4, and ages used for maximum depositional age determinations are shown in Figure 7. Fm, Formation; MDA, maximum depositional age; Mtn, Mountain; NV, Nevada; UT, Utah.

eruptions [6, 17, 35, 124, 125]. The tight age constraints that we obtained for many of the strata discussed here (Figure 3), as well as the upward-younging MDAs observed in some sections (Figures 4 and 8), suggest short lag times between zircon crystallization and deposition. We therefore interpret many of these zircon MDAs to approximate true depositional ages (see References 3, 35).

3. Results and Interpretations: Characteristics of Prevolcanic Cenozoic Sedimentary Successions in and Near Southern Nevada

In this section, we first discuss the most general constraints on depositional age for prevolcanic Cenozoic sedimentary rocks in southern Nevada and adjacent areas (Figure 2). We then present descriptions and depositional age control for twelve stratigraphic sections, including two that we did not sample as part of this study (Figure 4). Finally, we describe the patterns of prevolcanic Cenozoic sedimentation across the study area revealed by analysis of these sections.

3.1. Region-Wide Depositional Age Constraints. In most places, the *minimum* depositional age of each prevolcanic section is definitively constrained by the age of an overlying tuff (Figures 3 and 4). Across most of the study area (Figure 2), the oldest tuffs are ca. 27.6 Ma, but ages vary toward the margins of the study area and can reach up to 10 m.y. older or younger in certain areas. Specifically, the Monotony Tuff was the first locally erupted volcanic unit in most (but not all) sections [39, 123, 126; this study]. As can be seen in Figure 5 and online supplementary Table S1, five of the six volcanic samples that we analyzed (21JLS006, 20JLS061, 20JLS052C, 20JLS044, and 20JLS041) returned $^{40}Ar/^{39}Ar$ ages nearly identical to the 27.57 ± 0.04 Ma age of the Monotony Tuff established by Best et al. [126]. Using all seventy-nine preferred analyses for these five samples, we

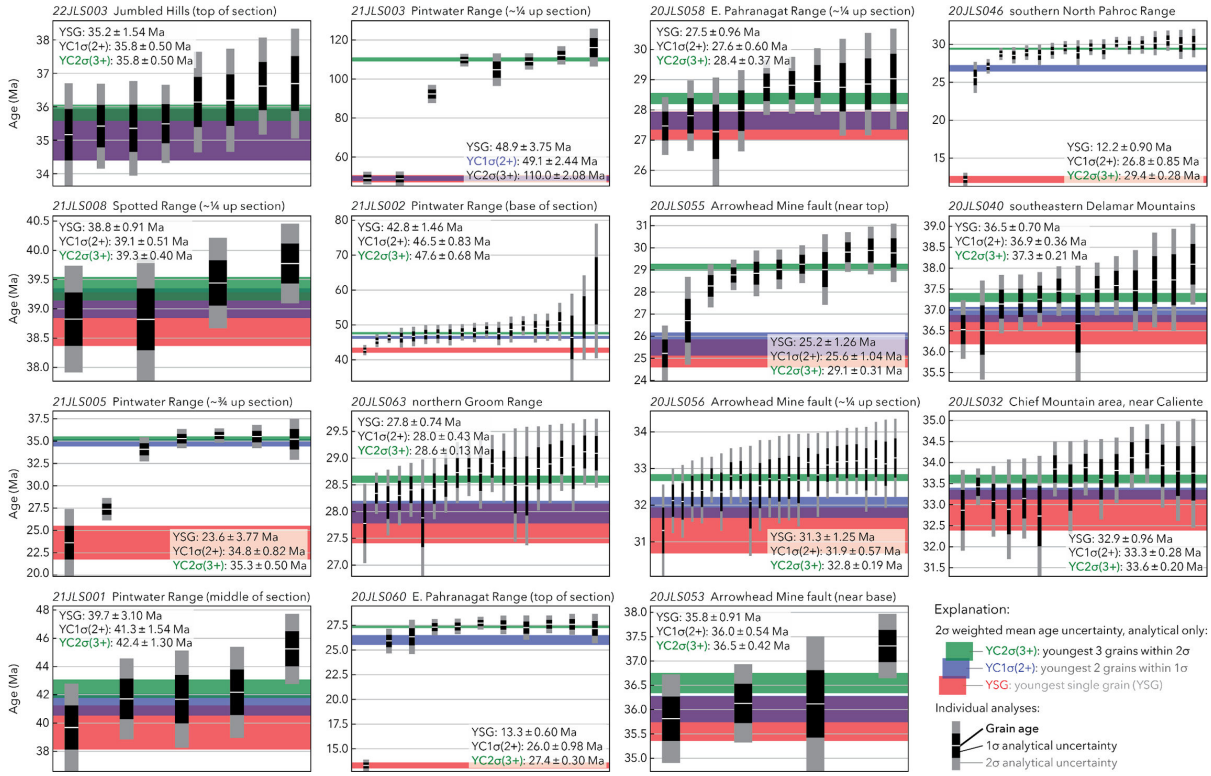

FIGURE 7: Detrital zircon maximum depositional ages (MDAs) ordered as in Figure 6. MDA uncertainties are reported at the 2σ level and only include internal (analytical) errors. In the text and Table 1, MDAs are reported using the preferred YC2σ(3+) method, and uncertainties are fully propagated (analytical and external) and reported at the 2σ level. Section locations are shown in Figure 2. Sample stratigraphic positions are shown in Figure 4.

obtained a weighted mean age of 27.60 ± 0.03 Ma, which we regard as an alternative eruptive age for the Monotony Tuff.

Besides increasing northward (Figure 1), volcanic ages increase slightly to the east at the latitude of our study: near the Nevada–Utah border, the oldest Cenozoic volcanic units are part of the ca. 27.9 Ma and younger Isom Formation [27, 123, 127]; in parts of southwestern Utah, the oldest volcanic rocks are the ca. 29–28 Ma Lund Formation and ca. 30.1 Ma Wah Wah Springs Formation of the Needles Range Group, as well as tuffs of the ca. 37–33 Ma Brian Head Formation [27, 28, 88, 123, 128]. In contrast, the first definitively local volcanic rocks in the western parts of the study area and to the south of the study area are much younger, typically early to middle Miocene in age (ca. 16–15 Ma), including in the Grapevine-Funeral Mountains, in areas south of Frenchman Flat, and in the Frenchman Mountain–Lake Mead area [31, 33, 37, 129].

A fundamental constraint on the MDAs of these deposits is the age of underlying strata. Rocks below the base-Cenozoic unconformity vary dramatically in age (Figure 4); in southern Nevada and southeastern California, the underlying rocks span the Neoproterozoic and Paleozoic [38], whereas they are as young as the Late Cretaceous in the area of the Sevier fold-and-thrust belt (Figure 1) in southwestern Utah [27, 28, 130]. As we describe below, precise MDAs within prevolcanic Cenozoic successions in and near the study area have been published only for the Grapevine–Funeral Mountains area of southeastern California and southwestern Nevada [4, 6, 35], the Frenchman Mountain–Lake Mead area east of Las Vegas [50–52 and 124], and certain parts of southwestern Utah [27, 28]. Our new detrital zircon MDAs (Figure 7) provide tight age constraints for most of the sections that we studied (Figure 4). Below we describe each section (Figure 4) with preliminary interpretations of depositional environments and descriptions of new and published age data.

3.2. Age Control and Description of Southern Nevada-Area Stratigraphic Sections

3.2.1. Titus Canyon Area, Grapevine–Funeral Mountains, California–Nevada Border Area. In the Grapevine–Funeral Mountains and nearby areas along the California–Nevada border (Figure 2), the Eocene–Oligocene Titus Canyon Formation and equivalents are exposed discontinuously over the base-Cenozoic unconformity. The Titus Canyon Formation varies dramatically in thickness, but it is ~500 m thick in its reference section (Figure 4(a)) in the eastern Grapevine Mountains [4, 6, 30, 33, 37, 131]. There, the unit is unconformably overlain by ~400 m of the early to middle Miocene Panuga Formation and ~500–850 m of reworked volcanic rocks of the middle Miocene Wahguye Formation, which are themselves overlain by the first local volcanic rocks, erupted ca. 15–14 Ma [6, 33, 37]. Deposition of the Titus Canyon Formation probably began slightly before 38

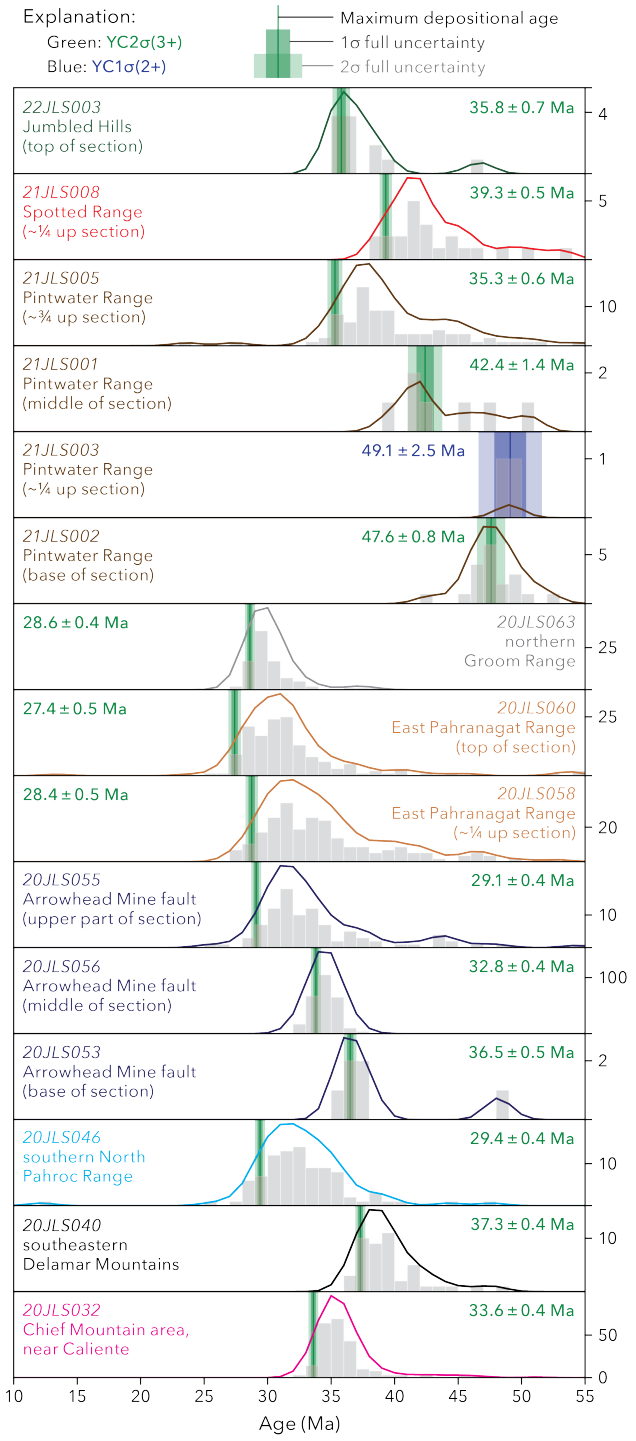

FIGURE 8: Kernel density estimates (KDEs) for the youngest grains in sedimentary samples analyzed for U-Pb zircon ages. All maximum depositional ages (MDAs) were determined from the weighted mean of the youngest three grains that overlap within 2σ uncertainty (YC2σ[3+], shown in green), except for the MDA for sample 21JLS003, which was determined from the youngest two grains that overlap within 1σ uncertainty (YC1σ[2+], shown in blue). Reported 2σ errors of the MDAs include both analytical and external uncertainties, as explained in the text. Sample 20TS49 is not shown because it yielded no Cenozoic ages. Histogram bin size and KDE bandwidth are 1 m.y.

Ma [4, 6, 132], which is around the same age as the base of many of the sections we studied in southern Nevada (see below). Deposition of the unit as defined by Miller et al. [6] continued until ca. 24–22 Ma, later than the ca. 28–27 Ma tuffs that define the tops of the other sections (Figures 2 and 4).

Refining prior work [30], Miller et al. [6] and Midttun et al. [4] identified three informal lithostratigraphic members within the Titus Canyon Formation. The 0–30-m-thick basal breccia member is overlain by the up to 300-m-thick red bed member, composed of siltstone, arkosic sandstone, and pebble-to-boulder conglomerate (Figure 4(a)). The upper part of the red bed member was deposited ca. 38–37 Ma, based on the presence of early late Duchesnian mammal fossils, but a meaningful MDA has not been established for the basal breccia member and the lower part of the red bed member [4, 6, 132]. The red bed member is overlain by the variegated member [4], which is an overall upward-fining succession of conglomerates containing well-rounded pebbles and cobbles and interbedded sandstones, calcareous siltstones and marls, and silty lacustrine limestone. Detrital zircon MDAs decrease upward (Figure 4(a)) from ca. 36 Ma near the base of the variegated member to ca. 24–22 Ma near its top [4, 6].

Midttun et al. [4] interpreted the upward-fining succession recorded by the variegated member to represent a transition from dominantly fluvial to lacustrine environments during the development of an extensional basin. Miller et al. [6] alternatively interpreted deposition in a fluvial system in which sediment largely bypassed the region. Miller et al. [6] found detrital clast compositions including red, radiolarian-bearing chert, black chert with phosphatic nodules, and reworked conglomerates themselves containing orthoquartzite and fine-grained mafic volcanic clasts, which they interpreted to indicate transport via south-flowing river systems from successions associated with the Golconda and Roberts Mountains allochthons some 300 km to the north in central Nevada (Figure 1).

3.2.2. South of Frenchman Flat. About 100 km to the southeast of the Grapevine–Funeral Mountains, in the southwestern Spotted Range, and to the south and southwest of nearby Frenchman Flat (Figure 2), a thick succession of Cenozoic rocks (Figure 4(b)) was deposited above upper Paleozoic carbonates [84]. Barnes et al. [84] identified a gentle angular unconformity within this succession, below which they assigned strata to the Horse Spring Formation and above which they assigned strata to the informal rocks of Pavits Spring. Ages are not well established for either unit, but Barnes et al. [84] reported a K-Ar biotite age of ca. 29 Ma in a tuffaceous interval of the Horse Spring Formation. Locally erupted volcanic rocks are notably not mapped in this area; these strata are instead overlain by Neogene(?) to Quaternary basin fill. Although the Monotony Tuff (the lowest volcanic unit deposited in many of the other sections that we studied) is not present [126], the possibility that its clasts

may be within the rocks of Pavits Spring [84] suggests a depositional age for that overlying unit of younger than ca. 27.6 Ma.

The lack of precise age control presents challenges for determining if any portion of this succession should be assigned to the prevolcanic or pre-ca. 17 Ma strata that are the focus of this study (Figure 3). Because of the unconformity between the two units and the larger proportion of volcanic material observed in the rocks of Pavits Spring, ignimbrite flare-up volcanism may have reached this latitude (but not this specific area) following deposition of rocks assigned to the Horse Spring Formation but before the rocks of Pavits Spring. Because the Horse Spring Formation name refers to rocks exposed east of Las Vegas [51], we tentatively designate rocks around the Spotted Range that were previously mapped as the Horse Spring Formation to the unnamed prevolcanic unit (Tso in Figure 4).

Although we were not able to visit these exposures within the NNSS (Figure 2), mapping and cross sections by Barnes et al. [84] indicate thicknesses ranging from ~200 m to at least 500 m for the Horse Spring Formation. Barnes et al. [84] described their Horse Spring Formation as dominantly argillaceous and silty limestones with lenses of conglomerate up to 30-m-thick and up to 9-m-thick intervals of reworked ash-fall tuffs. Conglomerate clasts are up to 30 cm and include quartzite and lesser carbonate within a clay-rich and tuffaceous sandstone matrix. Barnes et al. [84] suggested that clasts of Stirling Quartzite were transported from the north of the NNSS.

3.2.3. Northern Spotted Range and Fallout Hills. Roughly 30 km to the northeast, a thick, upward-fining succession of Cenozoic clastic and carbonate rocks is exposed around the northern flanks of the Spotted Range and Buried Hills and across most of the Fallout Hills (Figures 2 and 4(c)). These strata were deposited over early and late Paleozoic rocks that, respectively, comprise the upper and lower plates of the Spotted Range thrust [38, 40, 81, 83]. Apparent depositional contacts between Cenozoic and older rocks and variations in unit thickness (subtly visible in Figure 9) suggest deposition of Cenozoic rocks into an areally extensive depocenter characterized by tens to hundreds of meters of local paleorelief, likely related to erosion along lithological or structural zones of weakness [133]. We calculated a minimum stratigraphic thickness of ~1.5 km where we accessed this unit along two transects on the northeastern flanks of the Spotted Range (Figures 2 and 9). Our estimate is complicated by normal and strike-slip faults that cut the section, but distinctive patterns on satellite imagery (Figure 9) allow the stratigraphy to be correlated.

Tan sandstone (sample 21JLS008) within dominantly pebble and cobble conglomerates roughly 350 m above the base of the unit (Figure 10(a)) yielded a detrital zircon age spectrum consisting of about half (56%) Proterozoic ages (Figure 6), of which most (35% of the total) are Mesoproterozoic, with lesser proportions of Cenozoic (~8%), Mesozoic (~17%, dominated by Cretaceous), Paleozoic (~11%), and Archean (~7%) grains. This sample yielded an MDA of 39.3 ± 0.5 Ma from a weighted mean of four grains (Figure 7). An ignimbrite sampled from ~100 m above the sedimentary succession (21JLS009), across another recessive zone that likely contains the ca. 27.6 Ma Monotony Tuff [126], yielded a $^{40}Ar/^{39}Ar$ weighted mean age of 26.94 ± 0.02 Ma based on the weighted mean of thirteen sanidine dates (Figure 5). That age is statistically indistinguishable from a published age of 26.98 ± 0.04 Ma for the Coyote Summit Tuff, which is the lowest member of the Shingle Pass Formation [126].

The lower half of the succession is dominantly pebble and cobble conglomerate with sandstone interbeds (Figures 10(b), 10(c), and 10(f)). Conglomerate clasts are subrounded to rounded and contain quartzite, lesser amounts of carbonate, very fine-grained silicious lithologies, and lithic sandstones (Figure 10(c)). Red, black, tan, and greenish chert are also present. The lenticular shape of sandstone beds with scoured bases and the presence of trough cross-beds and imbricate clasts suggest deposition in fluvial environments [134]. Occasional intervals of recessive mudstone and siltstone with lesser sandstone that range from meters to tens of meters thick are visible as yellowish stripes on gently rolling hills (Figures 9 and 10(a)). Sample 21JLS008 was collected from slightly below this more recessive interval, and access restrictions prevented us from reaching the lower 20% (~350 m) of the unit below that sample. However, the lowest portion of the section is likely also dominated by a conglomerate with interbedded sandstones based on its similar weathering appearance to the interval we studied. The upper half of the succession is overall finer-grained and carbonate-rich, but it likewise displays a range of clast sizes and facies. That interval is dominated by silty lacustrine carbonate, with interbedded mudstone, well-sorted sandstone, and pebble-to-cobble conglomerates with dominantly subrounded to rounded clasts that are occasionally imbricated. We interpret that the upper half of the succession was deposited in a lacustrine setting bordered by higher-energy environments including alluvial fans and rivers or streams. The composition of these coarser sediments suggests local sources in bounding uplands, although we cannot rule out input from outside the basin.

3.2.4. Eastern Pintwater Range. Approximately 15 km to the southeast, on the eastern flanks of the Pintwater Range (to the east of Gravel Canyon), a ~1-km-thick succession of prevolcanic Cenozoic strata rests unconformably on mostly Cambrian and Ordovician rocks (Figures 2 and 4(d)). Cenozoic rocks were likely deposited over at least tens of meters of paleorelief in the immediate area of the studied section, based on map patterns and field observations of apparent onlap of the lowest tens of meters of strata (see annotated satellite image in online supplementary material Figure S2). This section is similar to that near the Spotted Range (described above) in terms of its thickness, lithofacies, upward fining character, and clast types. The base of the unit contains mostly clast-supported pebble-to-boulder conglomerate with rounded to angular clasts

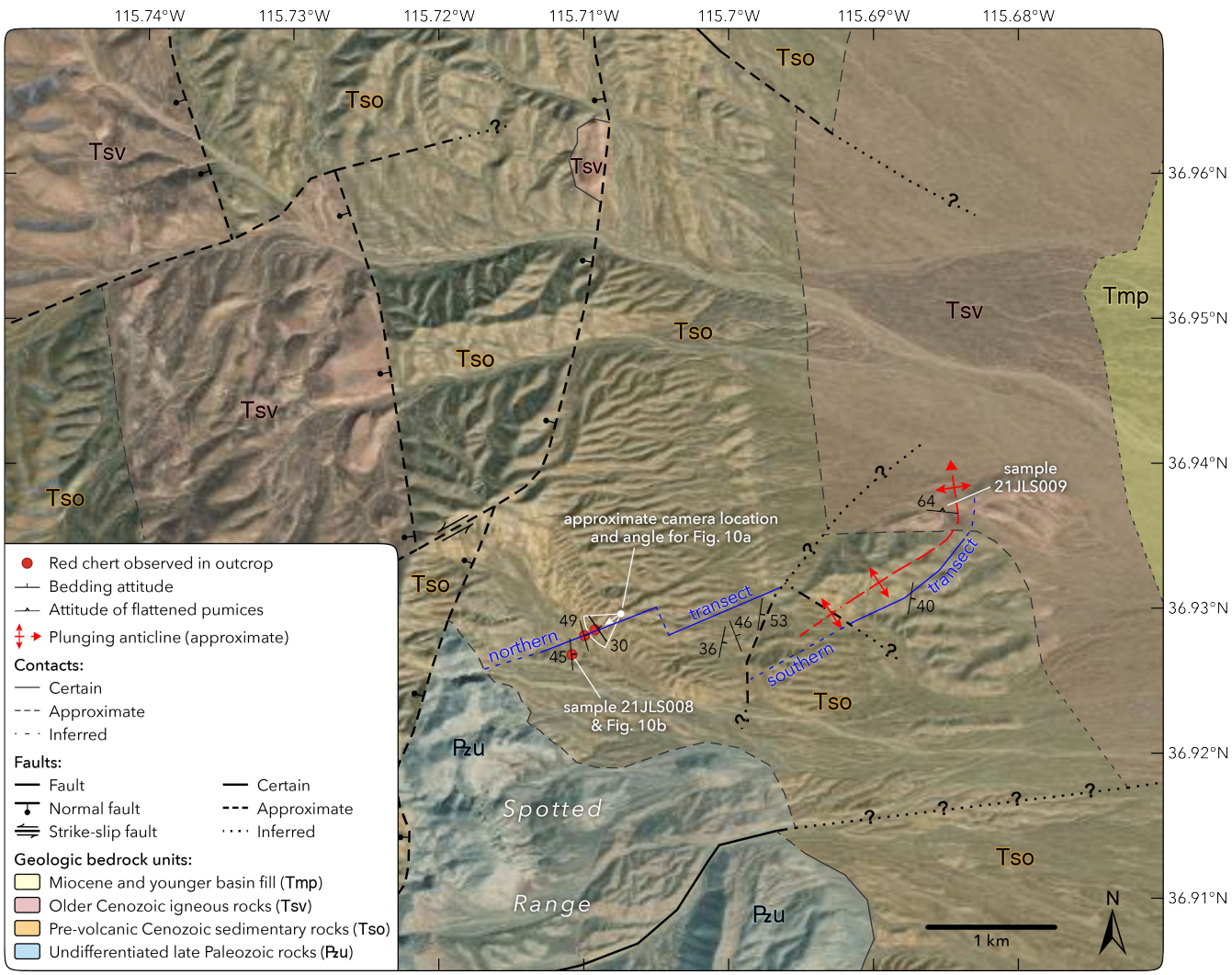

FIGURE 9: Reconnaissance bedrock geologic map of Cenozoic units on the northeastern flanks of the Spotted Range, southern Nevada. Bedrock units are projected under Quaternary cover, which is not mapped. Map location is shown in Figure 2, and stratigraphy along both transects is shown in Figure 4(c). The imagery is from Maxar Technologies. Mapping is updated from prior work [36, 38, 40, 83, 92] based on satellite imagery and new fieldwork (this study).

(Figure 10(g)), the largest of which exceed 1 m in diameter. Carbonate clasts, some of which resemble the underlying early Paleozoic carbonate lithologies, are dominant. However, the proportions of quartzite and sandstone clasts increase upward, and the proportion of boulder-size clasts decreases. Carbonate clasts are typically more angular than quartzite clasts, and clasts overall become more rounded upward. The first red chert clasts are observed around 200 m section height, and red, tan, and black chert pebbles are conspicuous at ~500 m (Figure 10(d)). The upper half of the section is more recessive, containing predominantly silty lacustrine limestone and carbonate-cemented sandstone and mudstone (Figure 10(e)), often containing pebble lags and intervals of pebble conglomerate with dominantly subrounded clasts.

We interpret this section to record a transition from deposition in basin-margin alluvial fans to lacustrine environments. We infer that carbonate clasts at the base were proximally sourced, whereas overlying quartzite and sandstone clasts were derived from more distal (but currently unknown) sources. The possible change in source areas may be reflected by modest changes in detrital zircon age spectra; two samples from the bottom ~250 m of the section (21JLS002 and 21JLS003) display prominent Jurassic (ca. 155–175 Ma) and Mesoproterozoic (ca. 1.0-1.5 Ga) peaks that are less prominent in samples from the upper half (21JLS001 and 21JLS005; Figure 5). The uppermost sample (21JLS005) contained the highest proportion of Cenozoic grains (34%), perhaps reflecting the approach of south-migrating Cenozoic eruptions.

Three of the four detrital zircon samples that we analyzed yielded upward-younging MDAs, from 47.6 ± 0.8 Ma for sample 21JLS003 collected ~10 m above the base of the unit to 35.3 ± 0.6 Ma for sample 21JLS005, about 220 m below the top (Figure 7). The exception was sample 21JLS003, at ~200 m section height, which yielded few Cenozoic grains and provided a less rigorous YC1σ(2+) age of 49.1 ± 2.5 Ma from two grains (Figure 7). The section is capped

FIGURE 10: (Three-page figure). (a) View of the northeastern flanks of the Spotted Range (Figure 2) looking toward the west-southwest (Figure 9). Prevolcanic Cenozoic sedimentary rocks labeled at the crest of the Spotted Range are separated from Paleozoic rocks by a normal fault system. (b) Sandstone displaying cross-bedding and soft-sediment deformation interbedded with a conglomerate in the
(Continued)

Figure 10: continued

Spotted Range section (Figure 4), approximately at the locality of sample 21JLS008. Stratigraphic up is toward the left. (c) Conglomerate clasts at ~350 m in the Spotted Range section. (d) Multi-colored chert pebbles in sandstone at ~550 m in the Pintwater Range section. (e) Truncated lacustrine limestone beds between sandstone ~200 m from the top of the Pintwater Range section. (f) Cross-bedded sandstone and pebble conglomerate at ~550 m in the Spotted Range section. (g) Boulder conglomerate and sedimentary breccia within 10 m of the base of the Pintwater Range section, near the location of sample 21JLS002. (h) Limestone containing algal laminations in the upper part of the northern Groom Range section, near the location of sample 20JLS063. (i) View to the east in the northern Jumbled Hills showing the lowest volcanic units and part of the underlying middle Cenozoic sedimentary succession. (j) Conglomerate clasts in the Jumbled Hills section. Image location is shown in panel i. (k) Sedimentary breccia containing almost exclusively carbonate clasts in the lowest exposure of the prevolcanic Cenozoic succession in the east-central East Pahranagat Range, about 15 m below the location of sample 20JLS058. (l) Diamictite within 10 m of the base of the prevolcanic Cenozoic strata in the southeastern East Pahranagat Range (Arrowhead Mine fault section), slightly below the level of sample 20JLS053. (m) Lacustrine carbonate with pebbles within the upper ~40 m of prevolcanic Cenozoic strata in the Arrowhead Mine fault section. (n) View toward the north of the oldest volcanic rocks and exposed portion of the underlying middle Cenozoic sedimentary succession near the southern tip of the North Pahroc Range. (o) Lacustrine carbonate in the upper part of the North Pahroc Range prevolcanic Cenozoic section. (p) Sandstone and pebble and cobble conglomerate with calcite-filled veins from the lower part of the prevolcanic Cenozoic sedimentary succession near Dodge Spring, in the Clover Mountains along the Nevada–Utah border. (q) Sedimentary breccia in the prevolcanic Cenozoic succession slightly west of Chief Mountain. carb, carbonate; ch, chert; qtzite, quartzite.

by the Monotony Tuff, which yielded a $^{40}Ar/^{39}Ar$ age of 27.57 ± 0.06 Ma (sample 21JLS006) based on five sanidine dates (Figure 5), in excellent agreement with the established age of that tuff [126]. Together, these samples constrain deposition to between ca. 47.6 and 27.6 Ma (Figure 4(d)).

3.2.5. Northern Groom Range. Some 80 km to the north-northwest of the Pintwater Range section (and about 60 km to the north-northwest of thick deposits in the Fallout Hills), a thinner prevolcanic Cenozoic succession is exposed on the northwestern flanks of the Groom Range (Figures 2 and 4(e)). Most of these deposits are inaccessible due to military restrictions, but upper strata that extend slightly onto public land are at least 50 m thick, and probable limestone cliffs are visible along strike on restricted lands (online supplementary material Figure S3). These upper strata are mostly bedded Cenozoic limestone containing white nodules but no obvious fossils (Figure 10(h)). Laminations of <1–2 cm thickness may be algal or due to precipitation of evaporite minerals. Although the basal contact is not exposed on public land, the unit was probably deposited over late Neoproterozoic and early Cambrian Wood Canyon Formation rocks [38]. The overlying ignimbrites have not been identified, but the oldest known in this area is the ca. 27.6 Ma Monotony Tuff [126].

We assign the observed (upper) portion of the unit an MDA of 28.6 ± 0.4 Ma based on a weighted mean of twenty-one grains (Figure 7) from sample 20JLS063, collected from a lens of pebble-bearing sandstone within a ~3-m-thick conglomerate interval that forms a scour within lacustrine limestone and is also overlain by limestone. Clasts within the conglomerate consist of dominantly angular to subrounded, dark gray carbonates. Twelve detrital zircon analyses were automatically excluded due to their extremely high U contents (U >2000 ppm), including seven that returned ages younger than ca. 27 Ma. The vast majority (84%) of grains are Cenozoic in age, and nearly all the remainder (14%) are Proterozoic (Figure 6).

3.2.6. Northeastern Jumbled Hills. About 35 km to the southeast of the northern Groom Range, prevolcanic Cenozoic deposits are exposed over a large portion of the Jumbled Hills, southeastern Groom Range, and northernmost Desert Range (Figures 2 and 4(f)), where they rest on strata ranging from Cambrian to Mississippian in age [36, 38–40]. Access is restricted over most of the area, but the top ~180 m of the unit is exposed on public land in the northeastern Jumbled Hills (online supplementary material Figure S4), above normal faults that have excised the lower part of the section (Figure 10(i)). The unit is capped by a light-gray, sanidine-poor ignimbrite that is likely the Monotony Tuff [39]. Based on total unit thickness estimates of at least 200 m determined from satellite imagery of access-restricted areas a few km to the south (online supplementary material Figure S4), these deposits may be contiguous beneath Emigrant Valley with those that cover the Fallout Hills.

The sedimentary succession contains 2–5-m-thick, alternating intervals of cross-bedded to featureless conglomerate, cross-bedded sandstone, and recessive, sandy red claystone that are separated by sharp bedding contacts (Figure 10(i)). No carbonates are exposed near the top, unlike in other sections. Conglomerate intervals are often clast-supported, and clasts range from subangular to rounded but are dominantly subrounded, with the largest tending to be more rounded and up to ~15 cm. Carbonates are the most common clasts, alongside lesser quartzite, siltstone, and black, red, and tan chert (Figure 10(j)). We interpret that the alternating clast-supported conglomerate, cross-bedded sandstone, and silty mudstone indicate deposition in a fluvial environment.

3.2.7. East-Central East Pahranagat Range. About 30 km to the east-northeast of the northeastern Jumbled Hills, in the east-central part of the East Pahranagat Range (Figures 2 and 4(g)), prevolcanic Cenozoic rocks rest unconformably atop Mississippian shale [39]. Although the base of the section is not clearly exposed, its location is constrained

within a few tens of meters (online supplementary material Figure S5), suggesting that the full unit thickness is not significantly greater than our minimum estimate of ~55 m.

This section displays a roughly upward-fining character. The lowest ~30 m of the section consists of a clast-supported conglomerate displaying crude, low-angle crossbedding. The conglomerate is composed of angular to subangular, pebble- to boulder-sized clasts up to 40 cm. Clasts are almost exclusively Paleozoic carbonates, some of which contain horn corals and crinoid fragments (Figure 10(k)). This interval contains several 2–5-m-thick upward-fining successions. The conglomerate becomes more matrix-rich upward, with clasts concentrated in discrete horizons. Above this is ~20 m of fossiliferous white and gray lacustrine carbonate with frequent interbeds of pebble and cobble conglomerate. The conglomeratic interbeds are markedly different from the conglomeratic beds below, with a whiter matrix and clasts that are smaller (up to only ~15 cm) and range between angular and rounded but are subangular on average. Clasts in this interval include not only gray carbonate but also quartzite; pink, tan, and light gray carbonates; and dark brown metasiltstone. The uppermost ~5 m is light gray sandstone and red-weathering pebble and cobble conglomerate. We interpret this section to record a transition from basin-margin alluvial fans to lacustrine environments.

Detrital zircon samples of sandstones ~20 m above the base (20JLS058) and ~5 m from the top (20JLS060) of the prevolcanic unit (Figure 4(g)) yielded strikingly similar age spectra that suggest similar sediment sources (Figure 6); both are dominated by Cenozoic ages (61%–63%), much of the remainder is Proterozoic (27%–28%, divided about evenly between Paleoproterozoic and Mesoproterozoic, with only a small fraction Neoproterozoic), 8%–9% is Mesozoic, and very small proportions are Paleozoic or Archean. We determined detrital zircon MDAs (Figure 7) of 28.4 ± 0.2 Ma for the lower sample (20JLS058) and 27.4 ± 0.5 Ma for the upper sample (20JLS060), the latter of which is indistinguishable within error from our 27.61 ± 0.03 Ma $^{40}Ar/^{39}Ar$ age (Figure 5) for the capping Monotony Tuff (sample 20JLS061).

3.2.8. Arrowhead Mine Section, Southeastern East Pahranagat Range. About 15 km to the southeast of the east-central East Pahranagat Range section, a full prevolcanic succession is exposed on the south side of the Arrowhead Mine fault, on the southeastern flanks of the East Pahranagat Range (Figures 2 and 4(h)). The succession rests above an angular unconformity with early Paleozoic quartzites and carbonates (online supplementary material Figure S6) and is capped by the ca. 27.6 Ma Monotony Tuff [39, 94]. We measured the Cenozoic strata at a 10-cm scale, finding a thickness of ~120 m.

As with several others, this succession generally fines upward from conglomerates to limestones. The lowest ~25 m is pebble-to-boulder conglomerate and diamictite (Figure 10(l)), with a single ~1-m-thick limestone interbed. The proportion of sandstone and sandy diamictite increases upward in the lower ~25 m of the unit. Above this, the zone between ~25 and 60 m is mostly pebble-to-boulder conglomerate that is sometimes better sorted. Above a ~25-m covered interval, an intermittently silty to sandy tabular limestone (Figure 10(m)) with zones of algal laminations of 8–20 cm thickness comprises the uppermost ~40 m of the prevolcanic section. We interpret these facies trends to indicate a progression from mostly debris flow deposition in basin-margin alluvial fans to lacustrine environments.

Sediment composition appears to change only modestly up section. Diamictite at the base of the section is dominated by angular clasts of quartzite that resemble the immediately underlying Ordovician Eureka Quartzite [39, 94]. A few meters higher, between the levels of Figure 10(l) and sample 20JLS053 until ~25 m section height, conglomerates and diamictites contain slightly more rounded clasts (dominantly angular to subangular) of mostly gray limestone and lesser amounts of quartzite and brown limestone, as well as minor siltstone, perhaps indicating the introduction of a more distant sediment source. Although clast rounding continues to increase upward, with subrounded clasts dominant between ~25 and 60 m section height, clasts remain mostly carbonate with lesser quartzite and minor amounts of other lithologies. A lack of major provenance changes up section may also be indicated by the detrital zircon age spectra (Figure 6). Sample 20JLS053, from ~10 m section height, does not display distinguishably different pre-Cenozoic age peaks compared with a sample from the upper ~30 m of the unit (20JLS055). However, markedly different proportions of Cenozoic grains between these samples complicate direct comparisons, and a third sample (20JLS056), from ~25 m section height, yielded too few pre-Cenozoic ages (7% of the total) to provide meaningful information about pre-Cenozoic peaks.

The detrital zircon ages do, however, tightly constrain deposition of the prevolcanic Cenozoic unit in this section to beginning no more than ~10 m.y. before the first local volcanism (Figure 4(h)). Detrital zircon MDAs from the base, middle, and top of the succession young upward from 36.5 ± 0.5 to 29.1 ± 0.4 Ma (Figure 7 and Table 1). Together with the $^{40}Ar/^{39}Ar$ age of 27.63 ± 0.07 Ma for the capping Monotony Tuff (Figure 5 and online supplementary Table S1), deposition of the sedimentary succession is constrained between ca. 36.5 and 27.6 Ma, with the upper portion constrained to between ca. 29.1 and 27.6 Ma.

3.2.9. Southern North Pahroc Range. About 50 km to the north-northeast of the Arrowhead Mine fault section, Cenozoic sedimentary rocks are exposed near the southern tip of the North Pahroc Range (Figures 2 and 4(i)), where they are capped by a thick succession of volcanic tuffs. Although the unconformity between the base of this unit and the underlying Devonian Sevy Dolomite [40, 135] is obscured at the location of our section (Figure 10 and online supplementary material Figure S7), it is exposed only about 300 m to the southwest without obvious intervening faults [135], indicating a total unit thickness of only slightly greater

than the ~120 m calculated for the exposed portion of the section. Near that location, Scott et al. [135] mapped an ignimbrite of the Lund Formation slightly above the base of the Cenozoic succession and below the levels that we accessed (Figure 4(i)), which is probably the Lund Formation tuff [123]. Because the Lund Formation ignimbrite was erupted from a caldera only around 50 km to the northeast, this succession is best characterized as being largely deposited synchronously with (rather than before) nearby volcanism.

As with several others that we studied, this succession generally fines upward (Figure 4(i)). The bottom approximately one-third of the exposed portion is dominated by carbonate-cemented sandstone and pebble-to-cobble conglomerate. The presence in the float of up to 30-cm-wide clasts of Paleozoic quartzites and crinoid-bearing carbonates suggests recessive intervals of boulder conglomerate. Above the clastic interval, the unit is mostly lacustrine limestone (Figure 10(o)), containing minor sand and silt (<1% of total) but usually lacking cross-bedding or other indications of current flow. However, as noted by Scott et al. [135], recessive conglomerate intervals are present within the more resistant limestone. Within both the lower dominantly clastic and upper dominantly limestone intervals, we observed rare monomineralic clasts of euhedral quartz and biotite, possibly derived from ash-fall tuffs. We interpret these facies patterns to potentially indicate a transition from deposition in alluvial fans to an intermittently lacustrine environment, probably in the presence of rapidly changing topography during nearby volcanism. The Lund Formation ignimbrite that is exposed below the stratigraphic levels that we accessed [135] provides a minimum depositional age of 29.20 ± 0.08 Ma for most of the section (Figure 4(i)), based on the age established for that tuff elsewhere [123]. Together with a new $^{40}Ar/^{39}Ar$ age of 27.52 ± 0.08 Ma (sample 20JLS044) for the overlying Monotony Tuff (Figure 5), deposition of nearly all of the sedimentary succession at this location is tightly constrained to between ca. 29.2 and 27.6 Ma. A sandstone sample (20JLS046) collected from the top of the clastic interval (Figure 4(i)) does not further constrain the depositional timing for this unit as it yielded a detrital zircon MDA of 29.4 ± 0.4 Ma (Figure 7) that is within error of that of the underlying Lund Formation tuff.

Throughout the southern and central North Pahroc Range, Taylor et al. [136] and Scott et al. [135, 137] identified marked lateral changes in thickness within the lower part of this unit (their unit Tl). Within some of these rocks, exposed several kilometers to the east, northeast, and north of our section, they also identified numerous volcanic intervals besides the ca. 27.6 Ma Monotony Tuff and the ca. 29.2 Ma Lund Formation tuff, the lowest of which is the 31.13 ± 0.09 Ma [123] Cottonwood Wash Tuff. The apparent absence of most of the pre-Monotony Tuff volcanic intervals in the section we studied is likely related to the presence of topographic relief before and during deposition. Taylor et al. [136] and Taylor [138] interpreted the variable thicknesses of these sedimentary strata as well as the presence of a gentle (<10°) angular unconformity below the Monotony Tuff to be evidence of relief generated by multiple episodes of normal faulting, although the rocks could have also been deposited within paleovalleys and episodically dammed by volcanic rocks and local uplifts associated with volcanism.

3.2.10. Western Flanks of Chief Mountain, Near Caliente. In the northeastern part of the study area, about 35 km to the east-northeast of the North Pahroc Range section, a prevolcanic Cenozoic succession is exposed on the western flanks of Chief Mountain, northwest of the town of Caliente (Figures 2 and 4(j)). In this area, middle Cenozoic sedimentary rocks rest on late Neoproterozoic to Cambrian units across an angular unconformity. Although Rowley et al. [139] suggested that the unit varies in thickness from 0 to 30 m, we estimate a thickness of ~120 m at our section at approximately its thickest point in the area, based on map relations, field-measured dip angles, and satellite imagery (online supplementary material Figure S8). These sedimentary rocks are capped by Oligocene to Miocene volcanic rocks and lesser interbedded volcaniclastic deposits whose lowest unit over much of this area is the ca. 27.6 Ma Monotony Tuff [139].

The exposed sedimentary deposits consist chiefly of pebble-to-boulder conglomerate in a carbonate-cemented sandy matrix (Figure 10(q)). Lacustrine limestones were notably not observed, although exposures in this section are limited to discontinuous outcrops of resistant conglomerates. Clasts are dominantly subangular to rounded and are mostly dark gray carbonate as well as finely laminated, gray-pink carbonate and pink-red quartzite that resemble the lithologies exposed immediately beneath the unconformity, including the Stirling and Zabriskie Quartzites and the Wood Canyon and Highland Peak Formations [139]. We infer that this unit may have been deposited in an alluvial fan environment.

A sample of a well-sorted sandy matrix of pebble-to-boulder conglomerate (20JLS032) collected from ~40 m below the top of the unit (Figure 4(j)) yielded a detrital zircon MDA of 33.6 ± 0.4 Ma (Figure 7), bracketing deposition of these upper stratigraphic levels to ca. 33.6–27.6 Ma. That sample yielded mostly (76%) Cenozoic detrital zircon ages, with about 2% Mesozoic ages and most of the remainder (19%) split about evenly between the Mesoproterozoic and Paleoproterozoic (Figure 6).

3.2.11. Dodge Spring Area, Clover Mountains, Nevada–Utah Border. About 70 km to the southeast of the Chief Mountain section, in the Dodge Spring area of the Clover Mountains, on the Nevada–Utah border (Figure 2), Cenozoic sedimentary rocks rest unconformably above Triassic strata and are capped by volcanic rocks of the ca. 27.9 Ma and younger Isom Formation [27, 123, 127]. Although the unconformity at the base of the unit is not directly exposed (see satellite image in online supplementary material Figure S6), its stratigraphic top and bottom locations are well constrained between adjacent outcrops, and we estimate a unit thickness of ~90 m (Figure 4(k)). The true thickness may be somewhat greater based on suggestions by Anderson and Hintze [127] that the unit

may be structurally attenuated despite the absence of obvious faults.

Like several other sections described above, the lower portion contains mostly conglomerate and sandstone (Figure 10(p)). Conglomerate intervals often contain sandy lenses, and clasts are angular to rounded and range up to ~50 cm. The upper limestone interval (which contains cherty nodules) makes up a greater portion of this unit (~80%) than in most other sections. We infer that these strata reflect a transition from alluvial fan and/or fluvial to lacustrine deposition. Near our section, tuffs of the Isom Formation are interbedded within the upper part of the sedimentary unit, indicating that lacustrine deposition was coeval with the early stages of volcanism [127].

In the lower part of the section, clasts are dominantly carbonates, with lesser amounts of quartzite and black chert. Sample 20TS49 is from a red-colored, poorly sorted sandstone lens within pebble-to-cobble conglomerates in the bottom ~10 m of the unit. This sample yielded no Cenozoic zircon ages, so a Cenozoic MDA could not be established, but it yielded a broad distribution of ages between the Triassic and late Neoproterozoic (Figure 6) that is similar to those observed in the sample from the lower part of the Spotted Range section (21JLS008). Most (76%) grains yielded Proterozoic ages (dominantly Mesoproterozoic) that form a distinctive, continuous distribution with a peak at ca. 1.1–1.0 Ga and a gradual decline in frequency from ca. 1.1 to 2.0 Ga. The most similar Proterozoic age distributions are observed in the sample from the Spotted Range and, to a lesser extent, samples from the base of the Arrowhead Mine fault section (20JLS053) and from the southeastern Delaware Mountains (20JLS040).

At the location of our section, Anderson and Hintze [127] assigned these rocks an age of "Oligocene and Eocene?." Taylor [27] assigned correlative rocks to the Oligocene portion of the Claron Formation, which is the name applied to prevolcanic Cenozoic rocks near the Nevada–Utah border and throughout southwestern Utah. Throughout that area, the unit typically displays a progression of clastic rocks overlain by lacustrine limestone that is similar to what we observed for our section; that progression has been interpreted to suggest the presence of an Eocene lake in parts of southwestern Utah and an Oligocene age lake in easternmost Nevada [27]. The unit has been characterized in detail in much of this area [26–28], but few precise age constraints are available. Taylor [27] suggested that Claron Formation rocks increase in age to the southeast, from Oligocene in southeastern Nevada and near the Nevada–Utah border to Paleocene(?)–latest middle Eocene (an age established more recently by Biek et al. [28]) toward south-central Utah. The Claron Formation has been variously defined; some geologists have excluded volcanic rocks that were previously included within the upper part of the unit and assigned them instead to overlying strata, while others have included additional members at the bottom of the Claron Formation [27, 28, 140–142]. Because of this, as well as the potential for confusion arising from the unit's wide and diachronous Paleocene(?)–Oligocene age range (also see Reference 52), in Figure 4 we instead refer to these rocks using the more generic "Older sedimentary rocks" (Tso) name that we apply to other potentially correlative strata considered in this study.

3.2.12. Southern Delamar Mountains. About 35 km to the southeast of the Arrowhead Mine fault section, in the southern Delamar Mountains (Figures 2 and 4(l)), Cenozoic rocks were deposited unconformably over Carboniferous to Permian strata and are capped by the Monotony Tuff, which is itself overlain by a thick succession of Oligocene–Miocene ignimbrites [143]. These rocks were deposited over more than 100 m of paleotopographic relief, and their thickness varies from 0 to 150 m [143]. Although only the top ~10 m is exposed at the location of our section, we estimated a total unit thickness of at least 120 m for nearby exposures based on satellite imagery (online supplementary material Figure S10).

The exposed part of the unit is mostly clastic, containing pebble-to-boulder conglomerate and carbonate-cemented, bioturbated sandstone, as well as a 1–2-m-thick bed of sandy limestone. Clasts are subangular to rounded, range up to 4 cm, and include white and pink quartzites; brown and gray carbonates; red, brown, and tan chert; and carbonate clasts that include shell fragments and nonrounded rip-up clasts. Trough cross-stratification within the upper platy sandstone interval suggests deposition in fluvial environments [134]. Together, these lithologies may indicate a basin margin setting that experienced alternating fluvial, alluvial fan, and shallow lacustrine deposition.

A sandstone sample within a pebble conglomerate in the top ~1 m of the sedimentary unit (20JLS040) yielded a distribution of detrital zircon age peaks between ca. 1.0 and 1.9 Ga and minor Triassic, Jurassic, and early Paleozoic detrital zircon age peaks that together most closely resemble those obtained from the northeastern Spotted Range section (Figure 6). Deposition of this uppermost part of the sedimentary unit is constrained to between ca. 37.3 and 27.6 Ma, based on a detrital zircon MDA of 37.3 ± 0.4 Ma for this sample (Figure 7) and a $^{40}Ar/^{39}Ar$ eruptive age of 27.53 ± 0.16 Ma for a sample (20JLS041) of the overlying Monotony Tuff (Figure 5). This span of ~10 m.y. between the MDA and the overlying tuff is unusually long compared with the upper parts of other sections that we studied, although the true age difference could be less.

3.3. Spatial Variability in Stratal Age and Thickness. As shown in Figure 11, the successions described above can be generalized into two classes based on their thickness and depositional ages. Figure 12 provides depositional age constraints for these sections. The thinner deposits are younger overall and close in age to the overlying volcanic rocks. Exposures of these strata are located toward the east and north of the study area (Figure 2), including near the northern Groom Range, East Pahranagat Range, southern North Pahroc Range, Chief Mountain, Clover Mountains, and southern Delamar Mountains (Figure 4(g)–(l)). These deposits are remarkably similar where we observed them, with most around 100 m thick (despite portions of some sections not being exposed) and having MDAs typically

no more than ca. 10 m.y. older than the capping volcanic rocks (Figure 12). Where available near the section tops, MDAs can be within 1–2 m.y. of the age of the overlying tuff (e.g., the northern Groom Range and around the East Pahranagat Range), although an MDA near the top of the unit in the southern Delamar Mountains is almost 10 m.y. older than the first tuff (Figure 4(l)). In the North Pahroc Range, ca. 31.1–27.6 Ma volcanic rocks of the nearby Indian Peak–Caliente caldera field [123] are interbedded with the earliest Cenozoic sedimentary strata in an area that was characterized by marked preexisting or developing topographic relief [135–137] (Figure 4(i)).

A second class of deposits (Figure 11) that is of greater but variable thickness is exposed toward the western parts of the study area, largely within restricted areas but also as far west as the Nevada–California border (Figures 2 and 4). Like the thinner deposits, MDAs for the upper parts of this thicker class of deposits are usually only a few m.y. older than the overlying volcanic rocks (Figure 12). In contrast, the base of these strata can be considerably older, as is demonstrated best for exposures near the Pintwater range that yielded middle and late Eocene MDAs. Near the Pintwater Range, these deposits are ~1.0 km thick, and an MDA near the base is ca. 48 Ma (Figure 4(d)). An MDA of ca. 35.3 Ma three-quarters of the way up section suggests that deposition continued until at least that time there and probably also in the adjacent ranges (where MDAs are not available near the section tops). On the northeastern flanks of the Spotted Range, the prevolcanic Cenozoic succession reaches ~1.5 km thickness, but the ages of the section are not as well established. The one age available for this section, a detrital zircon MDA of ca. 39 Ma, was obtained from a sample collected >300 m above the base (Figure 4(c)). Farther to the west, in the Grapevine–Funeral Mountains, the earliest volcanism occurred in the middle Miocene time, yet deposition of the Titus Canyon Formation was initiated much earlier, 38–37 Ma or before.

It is of course possible that deposition of these thicker strata in southern Nevada could have initiated later than the ca. 47.6 Ma MDA that we obtained from their base (Figures 4(b)-(d), 4(f), and 8). However, as discussed by Lund Snee and Miller [3] and Schwartz et al. [35] for similar deposits elsewhere in the region, middle Cenozoic zircon populations likely originated from large ignimbrite eruptions to the north that appear to have continuously supplied material to more southerly latitudes via ash fall. Moreover, the broadly southward-younging pattern of volcanism across the region (Figure 2) ensured that younger mineral populations would have been closer and therefore more available to the basin. Therefore, the broadly upward-younging pattern of MDAs in the sections we describe (Figures 4, 8, and 12), as well as others throughout the region [3, 4, 6, 17, 35], suggests that many of these MDAs may not significantly precede the actual time of deposition (<< 1 m.y.).

3.4. Commonalities in Facies Patterns. As illustrated in Figure 11, we observe striking consistency in the depositional facies patterns preserved in prevolcanic Cenozoic successions in and near southern Nevada (Figure 2) despite differences in MDAs (Figures 8 and 12) and thickness (Figure 4). To first order, albeit with several exceptions and marked heterogeneity at the scale of meters to tens of meters, individual sections transition upward from conglomerate and/or breccia containing mostly locally derived clasts, to conglomerate and sandstone containing higher proportions of nonlocal clasts, and then to finer-grained clastic lithologies and limestone.

These commonalities suggest that the first deposition in both the thick and thin sections may have occurred as debris flows along basin margins, either concentrated along hillslopes or distributed across alluvial fans, with intermittent reworking by fluvial systems. Through time, basin-margin environments transitioned to fluvial or lacustrine environments. The appearance of fluvial deposits is accompanied by the introduction of nonlocal sediment in many cases. An upward transition to usually silty lacustrine limestone in most (but not all) sections heralds the onset of ponding, usually within only a few million years before the deposits were blanketed by ignimbrites.

4. DISCUSSION

4.1. Early Cenozoic Basins of the Nevada Hinterland. Our new geochronology and characterization of middle Cenozoic sedimentary rocks provide an improved view of regional basin development across the extant Sevier hinterland before the onset of widespread Neogene extension. These data provide the first clear evidence that a sedimentary basin or basin system developed in southern Nevada within the ca. 20 m.y. before the arrival of south-migrating volcanism, with deposition continuing in some areas until immediately before or even during the first volcanism. Sedimentation was diachronous within a geometrically complex basin network.

The oldest detrital zircon MDAs obtained across the study area (Figure 8) indicate that basin filling began as early as middle Eocene time, based on a ca. 47.6 Ma detrital zircon MDA that we obtained from the bottom of these deposits near the Pintwater Range (Figure 4(d)), and continued until ca. 27 Ma in several parts of the study area (Figure 12). This deposition produced thick successions concentrated around the Fallout and Buried Hills and the Spotted and Pintwater Ranges (Figures 2, 4(b)–(d), and 4(f)), reaching ~1.5 km on the northeastern flanks of the Spotted Range (and possibly greater in restricted areas such as the Fallout Hills). Figure 1 shows an approximate outline of this early depocenter, which we refer to as the Fallout Hills basin after the location of its greatest areal exposure [38, 39]. Its northeastern margin may have been slightly northeast of the Jumbled Hills (Figure 2) because these deposits decrease in thickness to at least 200 m in the northern Jumbled Hills (Figure 4(f)) and then to tens of m in the nearby East Pahranagat Range. The southwestern margin may have been slightly to the south and west of Frenchman Flat, where deposits are apparently only ~100–

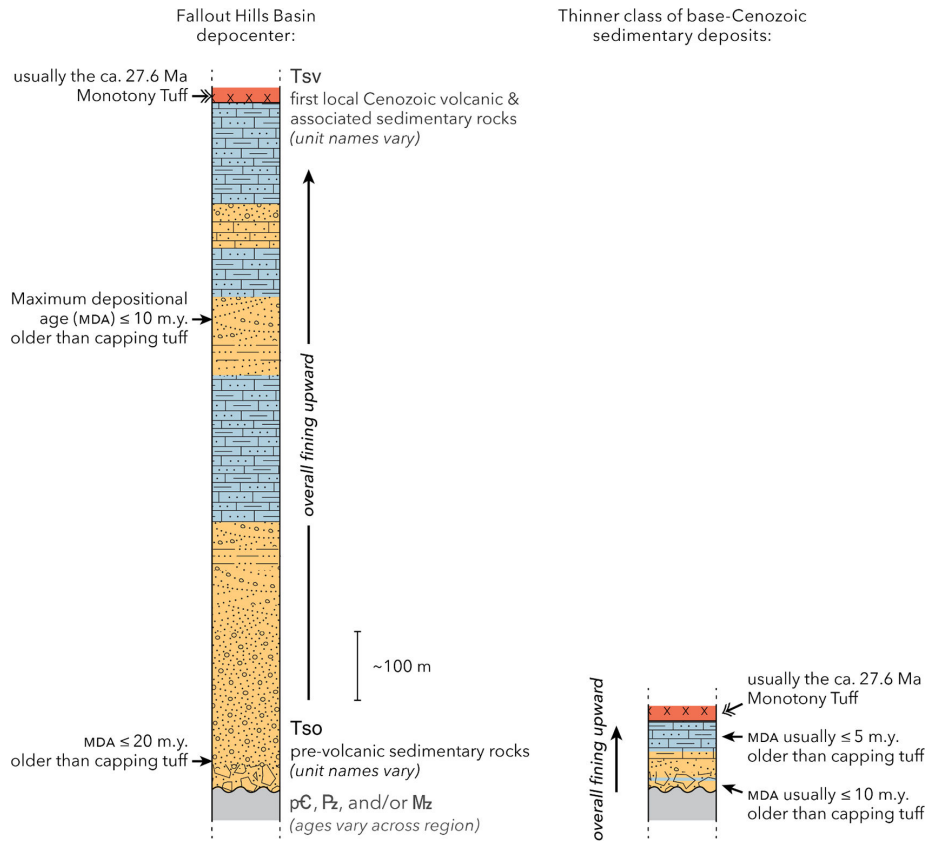

FIGURE 11: Generalized, characteristic sections of prevolcanic Cenozoic sedimentary rocks (labeled Tso) within the Fallout Hills basin (left), where they often exceed 1 km thickness, and elsewhere in southern Nevada and southwestern Utah (right), where they are usually ~100 m thick (Figures 1 and 2). Symbols are as given in Figure 4.

500 m thick (Figure 4(b)), although Cenozoic rocks in that area are difficult to correlate due to their poor age control.

Farther to the west, deposits of the Titus Canyon Formation in the Grapevine–Funeral Mountains (Figure 4(d)) likewise exceed 500 m, with considerable variability [4, 6, 33, 37]. It is unclear whether the two depocenters were contiguous, given the younger age of much of the Titus Canyon Formation (Figure 12) and the near absence of potentially correlative strata between there and the western flanks of the Spotted Range (Figure 2). Figure 1 does not show a basin in the area of the Grapevine–Funeral Mountains due to disagreement between Miller et al. [6] and Midttun et al. [4] regarding whether parts of the Titus Canyon Formation were deposited primarily in a lacustrine basin or via fluvial bypass (see above).

Generally, much thinner (around 100 m), isolated exposures of pre- and synvolcanic sedimentary rocks were deposited over a broader area of southern Nevada and southwestern Utah (Figure 2). Deposition of the thinner successions initiated later, in the latest Eocene to Oligocene time based on detrital zircon MDAs, and generally within about 10 m.y. before the eruption of the capping volcanic tuffs (Figures 8 and 12). Near and to the east of the Fallout Hills basin, the first capping volcanic rocks were erupted around 28–27 Ma [123, 126; this study], although up to ca. 31 Ma age tuffs are preserved within sedimentary successions near the North Pahroc Range, as noted above. Detrital zircon MDAs within the underlying sedimentary successions are typically ca. 38–37 Ma or younger (Figure 12). Figure 1 does not depict these deposits as significant sedimentary basins because their thin (<100 m) intervals of prevolcanic limestone (Figure 4) and generally isolated exposures (Figure 2) do not imply the presence of areally extensive basins (contrary to Reference 27).

Placed into their regional context, the sections we studied are among the southernmost of mostly isolated, sparsely distributed Cenozoic strata that were deposited in parts of the northern and central Basin and Range Province prior to, and in some cases synchronous with, the arrival of south-migrating ignimbrite flare-up volcanism (Figure 1). In the Copper Basin of northeastern Nevada (Figure 1), ~1.0 km of volcanic and interbedded sedimentary rocks of the Dead Horse Formation were deposited between ca. 45 and 37 Ma above the base-Cenozoic unconformity, indicating synchronous volcanism and sedimentation [11, 14, 15]. Slightly to the south within the Elko basin, deposition of up to ~850 m of Elko Formation rocks occurred between ca. 46 and 38 Ma, immediately preceding ca. 39–38 Ma and later magmatism [3, 17, 144–146]. In the nearby White Sage basin, thin (~150 m), dominantly lacustrine sedimentary strata were deposited below ca. 40 Ma capping volcanic rocks [13, 147]. Farther south, the Sheep Pass Basin of central Nevada (Figure 1) experienced deposition of ~1.0 km of Sheep Pass Formation sedimentary

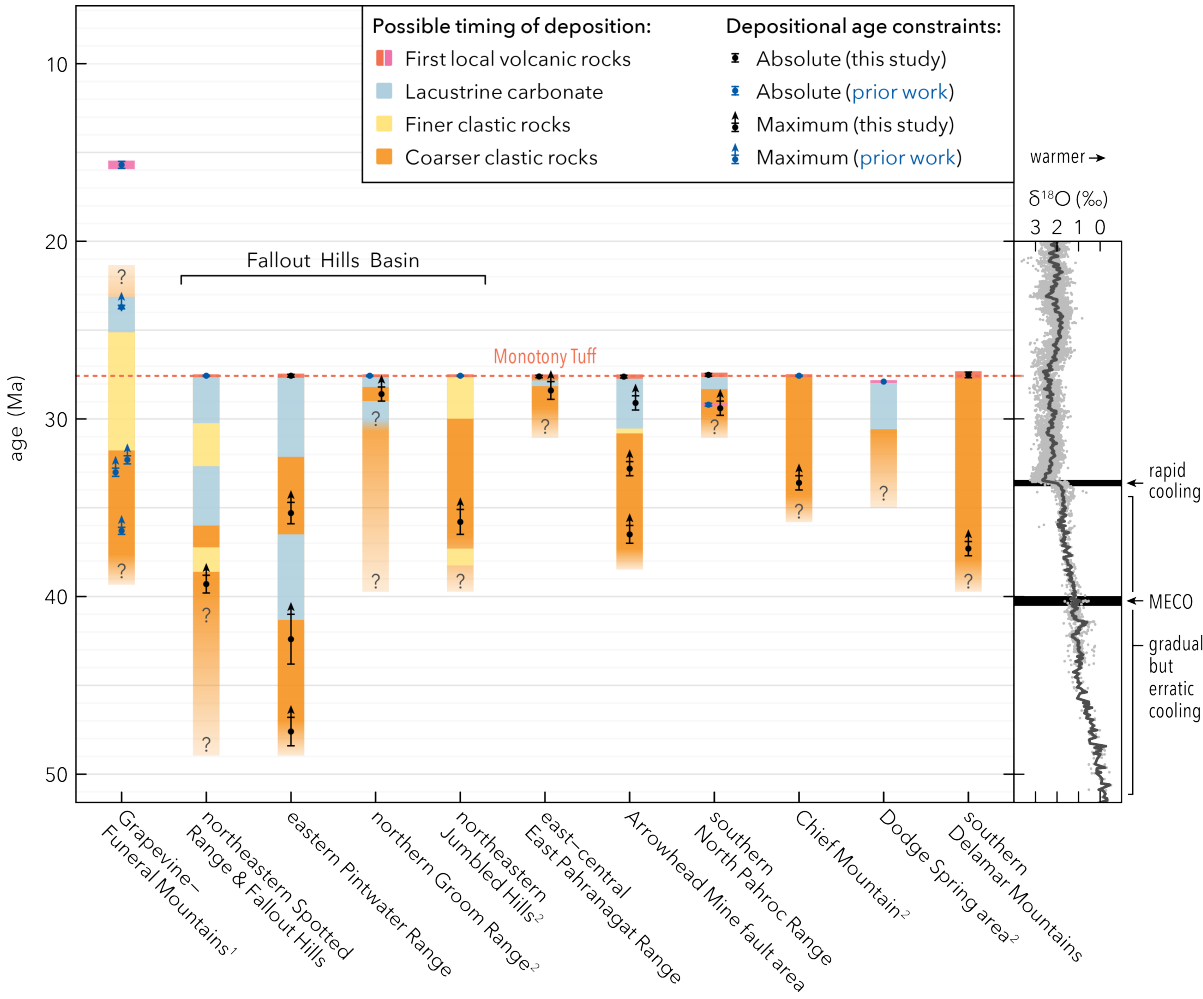

FIGURE 12: Permissible depositional age ranges of the studied prevolcanic Cenozoic sedimentary successions in southern Nevada (Figure 2) showing significant age constraints and stratigraphy simplified from Figure 4. Finer clastic rocks include siltstone and claystone with varying amounts of sand. Coarser clastic intervals include sandstone and conglomerate. Following convention, uncertainties for our U-Pb detrital zircon maximum depositional ages are 2σ and include the full analytical and external errors, whereas new $^{40}Ar/^{39}Ar$ feldspar minimum depositional ages are shown with their 2σ internal uncertainties (including uncertainties in *J* but not the ^{40}K decay constant), as described in the text. Uncertainties for published ages are as reported in the cited studies: 1—Snow and Lux [31] for minimum depositional age and Miller et al. [6] for maximum depositional ages; 2—Best et al. [123, 126]. Global pelagic $\delta^{18}O$ data are from Zachos et al. [158]. MECO—middle Eocene climatic optimum [165].

rocks in the latest Cretaceous and possibly later, followed by deposition of up to ~400 m of conglomerate, sandstone, siltstone, and limestone of the Sheep Pass Formation and Stinking Spring Conglomerate between ca. 38 and 35 Ma [21]. The sedimentary succession was capped almost immediately by volcanic rocks between ca. 36 and 35 Ma [21]. In nearby east-central Nevada, sedimentary rocks were deposited below the first volcanic rocks in several areas (not shown in Figure 1), usually <100 m but occasionally as much as 300 m thick [19, 21, 148]. Finally, to the south of the study area, ~150–250 m of Rainbow Gardens Formation strata were deposited between ca. 25 and 18 Ma in the Lake Mead area (Figure 2), before the unconformably overlying ca. 17 Ma and younger Horse Spring Formation extensional basin fill [50–52, 124, 125, 149–153]. Older Cenozoic sedimentary deposits are not documented to the south of the study area within the central Basin and Range Province [38], which could be due to nondeposition or removal during Miocene and younger uplift.

It is noteworthy that the ca. 47.6 Ma and younger Fallout Hills basin strata within the study area are partly synchronous with many of the other prevolcanic early to middle Cenozoic basin deposits that have been identified farther to the north in the extant Sevier hinterland (Figure 1). This study, therefore, shows that the network of Eocene sedimentary basins that developed over the Sevier hinterland prior to middle Cenozoic volcanism extended farther south than previously known. However, deposition in southern Nevada continued until ca. 27.6 Ma, whereas deposition in northern and central Nevada generally ceased by ca. 35 Ma or earlier (see References 3, 4). Farther south in the Rainbow Gardens basin (Figure 2), where Cenozoic sedimentation is not recorded before the latest Oligocene and the onset of magmatism was later than in the study

area, preextensional sedimentary deposition continued later still, until shortly before deposition of rapid and widespread extensional basin fill ca. 17 Ma [124].

4.2. Mechanisms of Basin Formation. Based on this and prior work, a picture is emerging of middle Cenozoic sedimentary deposition that occurred across the Basin and Range Province at the same time that several notable tectonic events affected the western United States (see References 3, 4). These events include changes in radial tractions above the inferred shallowly subducting Farallon slab [2, 154], the eventual removal of the slab from the base of the continent [91, 155], the approach of voluminous south-migrating ignimbrite flare-up volcanism (Figure 1) that is thought to have been caused by asthenospheric upwelling associated with slab removal [48, 156], protracted changes in plate convergence rates and the configuration of the Pacific–North America plate boundary to the west [157], and climatic changes that could have influenced erosion rates, sediment transport, and depositional facies [158, 159]. It has also been proposed that crustal thickening during Mesozoic shortening could have generated sufficient gravitational potential energy that it led to extension prior to widespread Neogene Basin and Range normal faulting [9, 160].

Although the overlapping timing of deposition in several of the sedimentary basins across Nevada that is discussed above (see Figure 1) could suggest a similar tectonic cause, it is challenging to link basin formation and filling with broader plate-scale processes due to pronounced differences in scale and, in some cases, incompatible timing. Many of the deposits that we document are only ~100 m thick and exposed in localized sections. Even up to ~1.5-km-deep Fallout Hills basin is too localized to directly relate to plate-scale processes. Moreover, prevolcanic sedimentary rocks are absent over much of the study area (Figure 2), with volcanic rocks deposited directly over the base-Cenozoic unconformity [36, 38–40, 80, 123, 126, 139, 143], indicating that either those areas were higher and sedimentary deposition did not occur there or any deposits were eroded away due to local changes in elevation prior to volcanism. In contrast, the predictions of many tectonic models that relate to the plate boundary or subduction system are at scales of hundreds to thousands of kilometers [154]. In addition, the development of accommodation within our study area cannot easily be linked with potential dynamic subsidence above the inferred shallowly subducting Farallon slab given modeling results suggesting that downward radial stresses developed substantially too early, in the Cretaceous, followed by modest uplift during the time that the studied successions were deposited [154], although other models predict modest subsidence during deposition of these sections [2]. Likewise, the similar age of onset for sedimentation in the Fallout Hills basin compared with basins farther north in Nevada, as discussed above (see also Figure 1), appears incompatible with a model of approximately south-propagating sedimentation linked to uplift or subsidence generated by removal of the Farallon slab [161]. If, however, subsidence associated with slab removal did contribute to sedimentation in the Nevada basins shown in Figure 1, then slab removal must have initiated at a similar time in both northern and southern Nevada and continued some 10 m.y. later, until ca. 27 Ma, in the study area, around the time when volcanism reached southern Nevada.

Instead of plate-scale processes driving basin formation, we suggest that the strata that we document in southern Nevada were mostly deposited in postcontractile basins whose locations and geometries were controlled by prior, late Sevier-era thrust faults, spatially variable fluvial incision, or nascent Cenozoic volcanism. It is also possible that older fluvial erosion that was concentrated along zones of structural or stratigraphic weakness generated accommodation for Eocene to Oligocene deposition. Beard [52] and Lamb et al. [124, 125] likewise concluded that most of the sediment deposited in the Rainbow Gardens basin to the southeast (Figure 2) was eroded from Paleozoic and Mesozoic rocks exposed on nearby topographic uplifts generated during Mesozoic to Paleogene Sevier and Laramide faulting and transported via younger Oligocene fluvial networks into an adjacent, northeast-trending lowland.

It is significant that the first Cenozoic strata in some parts of our study area were clearly deposited over appreciable paleotopographic relief (tens to hundreds of meters), as indicated by lateral variations in unit thickness and apparent bedding onlap above the base-Cenozoic unconformity in the northeastern Spotted Range (Figure 9), eastern Pintwater Range (online supplementary material Figure S2), North Pahroc Range (online supplementary material Figure S7) [135–137], and southeastern Delamar Mountains (online supplementary material Figure S10) [143]. The evidence that we document of hillslope and alluvial fan deposits in numerous sections likewise indicates deposition in areas of significant relief, and the spatial recurrence of such deposits signals the existence of rugged topography across the study area. Furthermore, it is noteworthy that the thickest deposits of the Fallout Hills basin are concentrated near exposures of the Spotted Range thrust fault system [38, 40, 79, 81, 83], including on the northern flanks of the Spotted Range where sedimentary rocks appear to fill a paleocanyon to the west across the Buried Hills and onto the upper plate of the thrust (Figures 2 and 9). Several other exposures of the prevolcanic Cenozoic rocks in southern Nevada are also located near exposures of Mesozoic thrust faults, including our sections in the southeastern Delamar Mountains, the East Pahranagat Range, and the Jumbled Hills (Figure 2).

Another contributor to accommodation in the sections we studied was likely the development of nearby magmatic centers, which Lund Snee and Miller [3] suggested would have profoundly affected topography and disrupted drainage networks. Although sedimentary rocks were deposited below volcanic rocks in all of the sections (Figure 4), the first eruptions of the Indian Peak–Caliente and Central Nevada ignimbrite fields, on the northern and northeastern sides of our study area (Figure 2), occurred ca. 36 Ma [123, 126], at approximately the time when

deposition initiated within several of the sections (Figure 12). In addition to regional-scale uplift associated with the addition of magma and thermal energy within the crust, localized topographic uplift and subsidence would have accompanied the filling and emptying of magma chambers, and early erupted material would have blocked drainage networks near the calderas, even if the material did not reach the studied sections. The likely influence of magmatism on accommodation and sedimentation is especially pronounced for the section in the southern North Pahroc Range, where marked topographic relief related to activity at the nearby Indian Peak–Caliente ignimbrite field (as discussed above) appears to have either predated or been synchronous with sedimentation [135, 137, 138]. The thickest and oldest successions within the study area, in the Fallout Hills basin depocenter, partially predate and were distal to these likely synvolcanic sediments and could have received increased sediment influx up section from developing topography to the north and east.

While it appears likely that the deposition we document occurred in accommodation left over from prior thrust faulting and created by synchronous development of magmatic systems, ponding indicated by the lacustrine limestone that we document near the top of many successions is consistent with several possible causes, including obstruction of outflow by either fault scarps, landslides, or newly erupted ignimbrites and lavas. However, we do not observe fanning dips or thickness changes that would indicate deposition in normal fault hanging walls, although such patterns would be challenging to observe, particularly for the thinner and less well-exposed sections. Even if some or all of these strata were deposited in accommodation created by normal faulting, the thickness and extent of these deposits do not indicate large-magnitude regional extension. Although encompassing a broad area and containing relatively thick (~1.5 km) deposits, even the Fallout Hills basin is spatially limited to one part of central Nevada, which is inconsistent with widespread regional extension. Although the later, thinner class of deposits extends over more of southern Nevada and into nearby areas (Figure 2), their isolated exposures and modest (~100 m) stratigraphic thicknesses would imply quite minor heaves along sparsely distributed normal faults. Moreover, the likelihood that deposition occurred over relict topography might be inconsistent with sedimentation due to active normal faulting because it would reduce the fault heaves required to explain the observed stratigraphic thicknesses. The localized sedimentation that we document across much of the study area in the middle Cenozoic time can be compared with the Neogene and later record of widespread extension, with accompanying basin fill covering vast portions of the Basin and Range Province and reaching over 3 km thickness in places [17, 52, 57, 162–164]. Finally, sediment weathering, flux, and accumulation rates and the resulting lithofacies could have been affected by gradual cooling and aridification punctuated by brief thermal events (such as the middle Eocene climatic optimum ca. 40 Ma [165]) that have been documented elsewhere in the western United States during the Eocene and Oligocene [159, 166], consistent with global trends (Figure 12) [158].

5. CONCLUSIONS

To better understand the surface dynamics active during the transition from Mesozoic and early Cenozoic shortening to later extension in the western United States (Figure 1), we conducted reconnaissance characterization and obtained radiometric age control for sections of middle Cenozoic strata throughout southern Nevada (Figure 2). These strata, deposited over the regional base-Cenozoic unconformity and underneath the first locally erupted volcanic rocks or the regionally extensive 17 Ma and younger extensional basin fill (Figure 3), form scattered and often poorly studied deposits. We find that a sedimentary basin system developed diachronously across parts of southern Nevada and adjacent areas beginning possibly as early as the middle Eocene, ca. 47.6 Ma or later. The earliest sedimentation occurred within a contiguous depocenter that we term the Fallout Hills basin (Figure 1), which extended across the Fallout, Buried, and Jumbled Hills and the Spotted and Pintwater Ranges. These strata reach at least 1.5 km thickness (Figure 4), and deposition continued until within 8 m.y. before they were blanketed by the first locally erupted volcanic unit, the ca. 27.6 Ma Monotony Tuff (Figure 12). It is unclear whether the partly synchronous (but mostly younger) Titus Canyon Formation of the California–Nevada border area was deposited into a contiguous westward extension of the Fallout Hills basin. A second class of prevolcanic sedimentation within the study area is characterized by much thinner (usually around 100 m) and apparently discontinuous deposits that are scattered across a broader area mostly to the east and southeast of the Fallout Hills basin. In sections that yielded MDAs, most of these strata were deposited within about 10 m.y. before the volcanic rocks that cap them (Figure 12). To first order (and with several exceptions), both the thicker and thinner deposits fine upward, often with coarse, locally derived clastic material at the base, finer clastic material at intermediate levels, and lacustrine limestone at upper levels (Figure 11).

These depositional patterns appear to be too localized to be attributed to plate-scale processes such as dynamic subsidence above the shallowly subducting Farallon slab [154] or subsidence as the slab was removed [161, 167]. Many sections are only ~100 m thick, and even the thicker deposits of the Fallout Hills basin are limited in their extent within south-central Nevada (Figures 1 and 2). It instead appears more likely that these rocks were deposited in accommodation created by differential surface uplift associated with approaching regional magmatism (see References 3, 6, 168–170) because they were deposited shortly before and in some cases synchronous with the first major volcanic eruptions slightly to the north and east (Figure 2). Some older deposition also likely occurred in relict relief from major Mesozoic and possibly younger thrust faults that are exposed adjacent to several of the thicker sections

(Figure 2). Rates of erosion and sediment transport may also have been affected by numerous climatic changes documented throughout the Paleogene [158, 159]. Although we cannot rule out the possibility that some of these strata were deposited within the hanging walls of localized normal faults, the observed depositional patterns are not consistent with regionally significant or large-magnitude extension.

Data Availability

All supporting data are available as a U.S. Geological Survey Data Release [95].

Conflicts of Interest

The authors declare no conflicts of interest.

Acknowledgments

GeoSep Services and ZirChron, LLC, conducted skilled mineral separation. We thank Daniel G. Alberts and Sarah W. M. George for their expertise and assistance with U-Pb zircon data collection at the University of Arizona LaserChron Center. We also thank Richard J. Moscati for assistance with $^{40}Ar/^{39}Ar$ sample preparation. The manuscript benefited from conversations with L. Sue Beard, Ryan E. Frazer, Amy K. Gilmer, Melissa (Lisa) A. Lamb, Karen I. Lund, Elizabeth L. Miller, Chester (Cal) A. Ruleman, and Ren A. Thompson. Constructive reviews by L. Sue Beard, Andrew V. Zuza, and an anonymous referee improved the manuscript. Any use of trade, firm, or product names is for descriptive purposes only and does not imply endorsement by the U.S. Government. Note that the first author's surname recently changed from Lund Snee to Lundstern. This paper cites works listing both author names. The U.S. Geological Survey National Cooperative Geological Mapping Program funded this work.

Supplementary Materials

The Supplementary Material includes one Supplementary Information file in .docx format and Supplementary Table S1 in .xlsx format. The Supplementary Information file includes the Supplementary Figures and associated references. The Supplementary Figures provide satellite photographs, schematic stratigraphic sections, and additional information for the stratigraphic sections that we sampled. Supplementary Table S1 provides results for $^{40}Ar/^{39}Ar$ and U-Pb geochronology.

REFERENCES

[1] L. J. Liu, "Rejuvenation of Appalachian topography caused by subsidence-induced differential erosion," *Nature Geoscience*, vol. 7, no. 7, pp. 518–523, 2014.

[2] A. Bahadori, W. E. Holt, R. Feng, et al., "Coupled influence of tectonics, climate, and surface processes on landscape evolution in southwestern North America," *Nature Communications*, vol. 13, no. 1, 2022.

[3] J.-E. Lund Snee and E. L. Miller, "Magmatism, migrating topography, and the transition from Sevier shortening to Basin and Range extension, western United States," in *Geological Society of America Special Paper 555: Tectonic evolution of the Sevier-Laramide hinterland, thrust belt, and foreland, and postorogenic slab rollback (180–20 Ma)*, J.P. Craddock, D.H. Malone, B.Z. Foreman, and A. Konstantinou, Eds., 2022.

[4] N. Midttun, N. A. Niemi, and B. Gallina, "Stratigraphy of the Eocene–Oligocene Titus Canyon Formation, Death Valley, California (USA), and Eocene extensional tectonism in the Basin and Range," *Geosphere*, vol. 19, no. 1, pp. 258–290, 2023.

[5] P. G. DeCelles, "Late Jurassic to Eocene evolution of the Cordilleran thrust belt and foreland basin system, western USA," *American Journal of Science*, vol. 304, no. 2, pp. 105–168, 2004.

[6] E. L. Miller, M. E. Raftrey, and J.-E. Lund Snee, "Downhill from Austin and Ely to Las Vegas: U-Pb detrital zircon suites from the Eocene–Oligocene Titus Canyon formation and associated strata, Death Valley, California," in *Geological Society of America Special Paper 555: Tectonic Evolution of the Sevier-Laramide Hinterland, Thrust Belt, and Foreland, and Postorogenic Slab Rollback (180-20 Ma)*, J.P. Craddock, D.H. Malone, B.Z. Foreman, and A. Konstantinou, Eds., 2022.

[7] M. G. Best, D. L. Barr, E. H. Christiansen, S. Gromme, A. L. Deino, and D. G. Tingey, "The Great Basin Altiplano during the middle Cenozoic ignimbrite flareup: insights from volcanic rocks," *International Geology Review*, vol. 51, nos. 7–8, pp. 589–633, 2009.

[8] C. P. Chamberlain, H. T. Mix, A. Mulch, et al., "The Cenozoic climatic and topographic evolution of the western North American Cordillera," *American Journal of Science*, vol. 312, no. 2, pp. 213–262, 2012.

[9] P. J. Coney and T. A. Harms, "Cordilleran metamorphic core complexes: Cenozoic extensional relics of Mesozoic compression," *Geology*, vol. 12, no. 9, 1984.

[10] C. D. Henry, N. H. Hinz, J. E. Faulds, et al., "Eocene-Early Miocene paleotopography of the Sierra Nevada-Great Basin-Nevadaplano based on widespread ash-flow tuffs and paleovalleys," *Geosphere*, vol. 8, no. 1, pp. 1–27, 2012.

[11] A. S. Canada, E. J. Cassel, A. J. McGrew, et al., "Eocene exhumation and extensional basin formation in the Copper Mountains, Nevada, USA," *Geosphere*, vol. 15, no. 5, pp. 1577–1597, 2019.

[12] J. F. Smith and K. B. Ketner, "Stratigraphy of post-Paleozoic rocks and summary of resources in the Carlin-Pinon range area, Nevada," *United States Geological Survey Professional Paper [Internet]*, 1976.

[13] C. J. Potter, R. F. Dubiel, L. W. Snee, and S. C. Good, "Eocene extension of early Eocene lacustrine strata in a complex deformed Sevier-Laramide hinterland, northwest Utah and northeast Nevada," *Geology*, vol. 23, no. 2, 1995.

[14] J. M. Rahl, A. J. McGrew, and K. A. Foland, "Transition from contraction to extension in the northeastern Basin and Range: new evidence from the Copper Mountains, Nevada," *The Journal of Geology*, vol. 110, no. 2, pp. 179–194, 2002.

[15] A. J. McGrew, K. A. Foland, and D. F. Stockli, "Evolution of Cenozoic volcanism and extension in the Copper Mountains, northeastern Nevada,"in *Geological Society of America Abstracts with Programs*, 39:p. 226, Geological Society of America, 2007.

[16] J.-E. Lund Snee and E. L. Miller, "Preliminary geologic map of Cenozoic units of the central Robinson mountain volcanic field and northwestern Huntington Valley," *Nevada Bureau of Mines and Geology Open File*, 42, 2015.

[17] J.-E. Lund Snee, E. L. Miller, M. Grove, J. K. Hourigan, and A. Konstantinou, "Cenozoic paleogeographic evolution of the Elko Basin and surrounding region, northeast Nevada," *Geosphere*, vol. 12, no. 2, pp. 464–500, 2016.

[18] T. D. Fouch, J. H. Hanley, and R. M. Forester, "Preliminary correlation of Cretaceous and Paleogene lacustrine and related nonmarine sedimentary and volcanic rocks in parts of the eastern Great Basin of Nevada and Utah," in *Basin and Range Symposium. Rocky Mountain Association of Geologists*, G. W. Newman, and H. D. Goode, Eds., pp. 305–312, 1979.

[19] P. B. Gans, G. A. Mahood, and E. Schermer, "Synextensional magmatism in the Basin and Range Province: a case study from the eastern Great Basin," *GSA Special Papers*, vol. 233, no. 1, pp. 1–53, 1989.

[20] K. Lund, L. S. Beard, and W. J. Perry, "Relation between extensional geometry of the northern Grant Range and oil occurrences in Railroad Valley, east-central Nevada," *AAPG Bulletin*, vol. 77, no. 6, pp. 945–962, 1993.

[21] P. Druschke, A. D. Hanson, and M. L. Wells, "Structural, stratigraphic, and geochronologic evidence for extension predating Palaeogene volcanism in the Sevier hinterland, east-central Nevada," *International Geology Review*, vol. 51, nos. 7–8, pp. 743–775, 2009.

[22] P. Druschke, A. D. Hanson, M. L. Wells, T. Rasbury, D. F. Stockli, and G. E. Gehrels, "Synconvergent surface-breaking normal faults of Late Cretaceous age within the Sevier hinterland, east-central Nevada," *Geology*, vol. 37, no. 5, pp. 447–450, 2009.

[23] A. R. Lechler and N. A. Niemi, "Sedimentologic and isotopic constraints on the Paleogene paleogeography and paleotopography of the southern Sierra Nevada, California," *Geology*, vol. 39, no. 4, pp. 379–382, 2011.

[24] K. E. Snell, P. L. Koch, P. Druschke, B. Z. Foreman, and J. M. Eiler, "High elevation of the 'Nevadaplano' during the Late Cretaceous," *Earth and Planetary Science Letters*, vol. 386, pp. 52–63, 2014.

[25] P. M. Goldstrand, "Evolution of Late Cretaceous and early Tertiary basins of southwest Utah based on clastic petrology," *SEPM Journal of Sedimentary Research*, vol. Vol. 62, no. 3, pp. 495–507, 1992.

[26] P. M. Goldstrand, "Tectonic development of Upper Cretaceous to Eocene strata of southwestern Utah," *Geological Society of America Bulletin*, vol. 106, no. 1, pp. 145–154, 1994.

[27] W. J. Taylor, "Stratigraphic and lithologic analysis of the Claron Formation in southwestern Utah," *Utah Geological Survey*, vol. 93, 1993.

[28] R. Biek, P. Rowley, J. Anderson, F. Maldonado, D. Moore, and D. Hacker, "Geologic map of the Panguitch 30' X 60' quadrangle, Garfield, Iron and Kane counties, Utah," *Utah Geological Survey Map* vol. 270DM, 2015.

[29] J. Sanjuan, A. Vicente, and J. G. Eaton, "New Charophyte flora from the Pine Hollow and Claron formations (southwestern Utah). taxonomic, biostratigraphic, and paleobiogeographic implications," *Review of Palaeobotany and Palynology*, vol. 282, 2020.

[30] M. W. Reynolds, "Stratigraphy and structural geology of the Titus and Titanothere Canyons area, Death Valley, California," Ph.D. thesis, University of California, Berkeley, California, 1969.

[31] J. K. Snow and D. R. Lux, "Tectono-sequence stratigraphy of Tertiary rocks in the Cottonwood Mountains and northern Death Valley area, California and Nevada," *Geological Society of America Special Paper 333: Cenozoic Basins of the Death Valley Region*, 1999.

[32] I. Çemen, L. A. Wright, and A. R. Prave, "Stratigraphy and tectonic implications of the latest Oligocene and early Miocene sedimentary succession, southernmost Funeral Mountains, Death Valley region, California," in *Geological Society of America Special Paper 333: Cenozoic Basins of the Death Valley Region*, 1999.

[33] C. J. Fridrich and R. A. Thompson, "Cenozoic tectonic reorganizations of the Death Valley region, southeast California and southwest Nevada," *US Geological Survey Professional Paper*, 2011.

[34] N. Niemi, "Geologic map of the central Grapevine Mountains, Inyo County, California, and Esmeralda and Nye Counties, Nevada," *Geological Society of America Digital Map and Chart Series 12*, 2012.

[35] T. M. Schwartz, A. K. Souders, J.-E. Lundstern, A. K. GIlmer, and R. A. Thompson, "Revised chronostratigraphy of Cenozoic strata on Bat Mountain, Death Valley region, California, USA, from zircon U-Pb geochronology," *Geosphere*, 2022.

[36] E. B. Ekren, P. P. Orkild, K. A. Sargent, and G. L. Dixon, "Geologic map of Tertiary rocks, Lincoln County, Nevada," *US Geological Survey IMAP*, 1977.

[37] N. A. Niemi, "Extensional tectonics in the Basin and Range Province and the geology of the Grapevine Mountains, Death Valley region, California and Nevada," Ph.D. thesis, California Institute of Technology, Pasadena, CA, 2002.

[38] J. B. Workman, C. M. Menges, W. R. Page, E. M. Taylor, E. B. Ekren, P. D. Rowley, et al., "Geologic map of the Death Valley ground-water model area, Nevada and California," . Miscellaneous Field Studies, *US Geological Survey*, 2002.

[39] A. S. Jayko, "Geologic map of the Pahranagat range 30' X 60' Quadrangle, Lincoln and Nye counties, Nevada," *U.S. Geological Survey Scientific Investigations Map 2904*, 2007.

[40] C. M. Tschanz and E. H. Pampeyan, Geology and mineral deposits of Lincoln County, Nevada *Nevada Bureau of Mines and Geology Bulletin*, vol. 73y, 1970.

[41] A. H. Lachenbruch and J. H. Sass, "9: Models of an extending lithosphere and heat flow in the Basin and Range Province," in *Geological society of America Memoirs 152: Cenozoic Tectonics and Regional Geophysics of the Western Cordillera*, R.B. Smith, and G.P. Eaton, Eds., pp. 209–250, 1978.

[42] G. P. Eaton, "The Basin and Range Province: Origin and tectonic significance," *Annual Review of Earth and Planetary Sciences*, vol. 10, no. 1, pp. 409–440, 1982.

[43] R. W. Saltus and G. A. Thompson, "Why is it downhill from Tonopah to Las Vegas?," *Tectonics*, vol. 14, no. 6, pp. 1235–1244, 1995.

[44] R. P. Kucks, "Bouguer gravity anomaly data grid for the conterminous US," in *US Geological Survey Digital Data Series DDS-9: National Geophysical Data Grids; Gamma-ray, Gravity, Magnetic and Topographic Data for the Conterminous United States*, J. D. Phillips, J. S. Duval, and R. A. Ambroziak, Eds., U.S. Geological Survey, Denver, CO, 1999.

[45] D. Blackwell, M. C. Richards, Z. S. Frone, J. F. Batir, M. A. Williams, A. A. Ruzo, et al, "SMU geothermal laboratory heat flow map of the Conterminous United States," 2011.

[46] J.-E. Lundstern and M. D. Zoback, "Multiscale variations of the crustal stress field throughout North America," *Nature Communications*, vol. 11, no. 1951, 2020.

[47] C. Kreemer, G. Blewitt, and W. C. Hammond, "Evidence for an active shear zone in southern Nevada linking the Wasatch fault to the Eastern California shear zone," *Geology*, vol. 38, no. 5, pp. 475–478, 2010.

[48] R. L. Armstrong and P. Ward, "Evolving geographic patterns of Cenozoic magmatism in the North American Cordillera: the temporal and spatial association of magmatism and metamorphic core complexes," *Journal of Geophysical Research*, vol. 96, no. B8, pp. 13201–13224, 1991.

[49] C. J. Rau and D. W. Forsyth, "Melt in the mantle beneath the amagmatic zone, southern Nevada," *Geology*, vol. 39, no. 10, pp. 975–978, 2011.

[50] R. E. Anderson, C. R. Longwell, R. L. Armstrong, and R. F. Marvin, "Significance of K-Ar ages of Tertiary Rocks from the Lake Mead region, Nevada-Arizona," *Geological Society of America Bulletin*, vol. 83, no. 2, 1972.

[51] R. G. Bohannon, "Nonmarine sedimentary rocks of tertiary age in the Lake Mead region, southeastern Nevada and northwestern Arizona," *U.S. Geological Survey Professional Paper 1259*, 1984.

[52] L. S. Beard, "Paleogeography of the Horse Spring formation in relation to the Lake Mead fault system, Virgin Mountains, Nevada and Arizona," in *Geological Society of America Special Paper 303: Reconstructing the History of Basin and Range Extension Using Sedimentology and Stratigraphy*, K.K. Beratan, Ed., pp. 27–60, 1996.

[53] J. K. Snow and B. P. Wernicke, "Cenozoic tectonism in the central Basin and Range: magnitude, rate, and distribution of upper crustal strain," *American Journal of Science*, vol. 300, no. 9, pp. 659–719, 2000.

[54] N. McQuarrie and B. P. Wernicke, "An animated tectonic reconstruction of southwestern North America since 36 Ma," *Geosphere*, vol. 1, no. 3, p. 147, 2005.

[55] J. E. Andrew and J. D. Walker, "Reconstructing late Cenozoic deformation in central Panamint Valley, California: Evolution of slip partitioning in the Walker Lane," *Geosphere*, vol. 5, no. 3, pp. 172–198, 2009.

[56] J. P. Colgan and C. D. Henry, "Rapid middle Miocene collapse of the Mesozoic orogenic plateau in north-central Nevada," *International Geology Review*, vol. 51, nos. 9–11, pp. 920–961, 2009.

[57] R. E. Anderson and L. S. Beard, "Geology of the Lake Mead region: an overview," in *Geological Society of America Special Paper 463: Miocene Tectonics of the Lake Mead Region, Central Basin and Range*, P.J. Umhoefer, L.S. Beard, and M.A. Lamb, Eds., pp. 1–28, 2010.

[58] C. D. Henry, A. J. McGrew, J. P. Colgan, A. W. Snoke, and M. E. Brueseke, "Timing, distribution, amount, and style of Cenozoic extension in the northern Great Basin." Edited by J. P. Evans and J. Lee *GSA Field Guide*, vol. 21, no. 2, pp. 27–66, 2011.

[59] T. S. Bidgoli, E. Amir, J. D. Walker, D. F. Stockli, J. E. Andrew, and S. J. Caskey, "Low-temperature thermochronology of the Black and Panamint mountains, Death Valley, California: implications for geodynamic controls on Cenozoic intraplate strain," *Lithosphere*, vol. 7, no. 4, pp. 473–480, 2015.

[60] C. P. Garrity and D. R. Soller, "Database of the geologic map of North America: adapted from the map by J.C. Reed, Jr. and others (2005)," in *US Geological Survey Data Series 424*, 2007.

[61] K. Lund, J. N. Aleinikoff, K. V. Evans, E. A. duBray, E. H. Dewitt, and D. M. Unruh, "SHRIMP U-Pb dating of recurrent Cryogenian and late Cambrian-Early Ordovician alkalic magmatism in central Idaho: implications for Rodinian rift tectonics," *Geological Society of America Bulletin*, vol. 122, nos. 3–4, pp. 430–453, 2010.

[62] F. G. Poole, J. H. Stewart, A. R. Palmer, C. A. Sandberg, R. J. Madrid, and R. J. Ross, "Latest Precambrian to latest Devonian time; Development of a continental margin," in *The Geology of North America: Cordilleran Orogen: Conterminous U.S*, Geological Society of America, Boulder, CO, 1992.

[63] J. H. Stewart, "Geology of Nevada," in *Nevada Bureau of Mines and Geology, Special Publication 4*, Geological Society of Nevada, 1980.

[64] J. G. Johnson and A. Pendergast, "Timing and mode of emplacement of the Roberts Mountains allochthon, Antler orogeny," *Geological Society of America Bulletin*, vol. 92, no. 9, 1981.

[65] D. W. Harbaugh and W. R. Dickinson, "Depositional facies of Mississippian clastics, Antler foreland basin, central Diamond Mountains, Nevada," *Journal of Sedimentary Research*, vol. 51, no. 4, pp. 1223–1234, 1981.

[66] A. H. Sallerand W. R. Dickinson, "Alluvial to marine facies transition in the Antler overlap sequence, Pennsylvanian and Permian of north-central Nevada," *Journal of Sedimentary Research*, vol. Vol. 52, no. 3, pp. 925–940, 1982.

[67] E. L. Miller, M. M. Miller, C. H. Stevens, J. E. Wright, and R. J. Madrid, "Late Paleozoic paleogeography and tectonic evolution of the western U.S. Cordillera," in *The Geology of North America: The Cordilleran Orogen: Conterminous US*, B.C. Burchfiel, P.W. Lipman, and M.L. Zoback, Eds., pp. 57–106, Geological Society of America, 1992.

[68] P. H. Cashman, J. H. Trexler, V. I. Davydov, and W. S. Snyder, "Tectonostratigraphy of the Great Basin from the Antler Orogeny through Pennsylvanian time," in *Great Basin Evolution and Metallogeny, Volume 1*, pp. 299–311, Geological Society of Nevada, Reno, NV, 2011.

[69] D. M. Sturmer, J. H. Trexler, and P. H. Cashman, "Tectonic analysis of the Pennsylvanian Ely-Bird Spring Basin: Late Paleozoic tectonism on the southwestern Laurentia margin and the distal limit of the Ancestral Rocky Mountains," *Tectonics*, vol. 37, no. 2, pp. 604–620, 2018.

[70] R. J. Leary, J. Quade, M. Read, and G. P. Wahlman, "Sedimentary record of late Paleozoic tectonism in the Monitor Range, central Nevada: implications for convergence along the western Laurentian margin," *Palaeogeography, Palaeoclimatology, Palaeoecology*, vol. 577, 2021.

[71] P. H. Cashman and D. M. Sturmer, "The Antler orogeny reconsidered and implications for late Paleozoic tectonics of western Laurentia," *Geology*, vol. 51, no. 6, pp. 543–548, 2023.

[72] B. C. Burchfiel, P. J. Pelton, and J. Sutter, "An early Mesozoic deformation belt in south-central Nevada-southeastern California," *Geological Society of America Bulletin*, vol. 81, no. 1, 1970.

[73] M. D. Carr, "Geometry and structural history of the Mesozoic thrust belt in the Goodsprings District, southern Spring Mountains, Nevada," *Geological Society of America Bulletin*, vol. 94, no. 10, 1983.

[74] M. A. Giallorenzo, M. L. Wells, W. A. Yonkee, D. F. Stockli, and B. P. Wernicke, "Timing of exhumation, Wheeler Pass thrust sheet, southern Nevada and California: Late Jurassic to Middle Cretaceous evolution of the southern Sevier fold-and-thrust belt," *GSA Bulletin*, vol. 130, nos. 3–4, pp. 558–579, 2018.

[75] S. Craddock Affinati, T. D. Hoisch, M. L. Wells, and S. Wright, "Retroarc Jurassic burial and exhumation of Barrovian metamorphic rocks dated by monazite petrochronology, Funeral Mountains, California," in *GSA Special Paper 555: Tectonic Evolution of the Sevier-Laramide Hinterland, Thrust Belt, and Foreland, and Postorogenic Slab Rollback (180–20 Ma)*, J. P. Craddock, D. H. Malone, B. Z. Foreman, and A. Konstantinou, Eds., 2022.

[76] R. L. Armstrong, "Sevier orogenic belt in Nevada and Utah," *Geological Society of America Bulletin*, vol. 79, no. 4, pp. 429–458, 1968.

[77] R. L. Armstrong, "Low-angle (denudation) faults, hinterland of the Sevier orogenic belt, eastern Nevada and western Utah," *Geological Society of America Bulletin*, vol. 83, no. 6, 1972.

[78] R. J. Fleck, "Tectonic style, magnitude, and age of deformation in the Sevier orogenic belt in southern Nevada and eastern California," *GSA Bulletin*, vol. 81, no. 6, pp. 1705–1720, 1970.

[79] J.-E. Lundstern, T. M. Schwartz, M. E. Berry, J. B. Workman, D. Woodring, P. L. Guth, et al, "Integrated 1:100,000-scale surficial and bedrock geologic mapping of the Indian Springs quadrangle, northwest of Las Vegas," *Geological Society of America Abstracts with Programs*, vol. 54, no. 5, 2022.

[80] P. D. Rowley, G. L. Dixon, E. A. Mankinen, K. T. Pari, D. K. McPhee, E. H. McKee, et al., "Geology and geophysics of White Pine and Lincoln counties, Nevada, and adjacent parts of Nevada and Utah: The geologic framework of regional groundwater flow systems," *Nevada Bureau of Mines and Geology Report*, vol. 56, 2017.

[81] C. R. Longwell, E. H. Pampeyan, B. Bowyer, and R. J. Roberts, "Geology and mineral deposits of Clark County, Nevada," *Nevada Bureau of Mines and Geology Bulletin*, vol. 62, 1965.

[82] P. L. Guth, "Geology of the Sheep Range, Clark County, Nevada," Massachusetts Institute of Technology [Ph.D. dissertation], Cambridge, MA, 1980.

[83] P. L. Guth, "Chapter 11: Superposed Mesozoic and Cenozoic deformation, Indian springs Quadrangle, southern Nevada," in *GSA Memoir 176: Basin and Range Extensional Tectonics Near the Latitude of Las Vegas, Nevada*, B.P. Wernicke, Ed., pp. 237–249, Geological Society of America, Boulder, Colorado, 1990.

[84] H. Barnes, E. B. Ekren, C. L. Rodgers, and D. C. Hedlund, "Geologic and tectonic maps of the Mercury quadrangle, Nye and Clark Counties, Nevada," in *US Geological Survey Miscellaneous Investigations Series Map I-1197*, 1982.

[85] W. R. Dickinson, M. A. Klute, M. J. Hayes, et al., "Paleogeographic and paleotectonic setting of Laramide sedimentary basins in the central Rocky Mountain region," *Geological Society of America Bulletin*, vol. 100, no. 7, pp. 1023–1039, 1988.

[86] T. F. Lawton, "Tectonic setting of Mesozoic sedimentary basins, Rocky Mountain region, United States," in *Society for Sedimentary Geology. SEPM (Society for Sedimentary Geology), Rocky Mountain Section*, M.V. Caputo, J.A. Peterson, and K.J. Franczyk, Eds., pp. 1–26, 1994.

[87] T. F. Lawton, "Chapter 12 Laramide sedimentary basins," in *Sedimentary Basins of the World, vol. 5*, A.D. Miall, Ed., pp. 429–450, 2008.

[88] R. Biek, P. Rowley, J. Hayden, D. Hacker, G. Willis, L. Hintze, et al., "Geologic map of the St. George and east part of the Clover Mountains 30' × 60' quadrangles, Washington and Iron counties, Utah," *Utah Geological Survey Map*, vol. 242DM, 2010.

[89] M. Fan and B. Carrapa, "Late Cretaceous–early Eocene Laramide uplift, exhumation, and basin subsidence in Wyoming: Crustal responses to flat slab subduction," *Tectonics*, vol. 33, no. 4, pp. 509–529, 2014.

[90] P. L. Heller and L. Liu, "Dynamic topography and vertical motion of the U.S. Rocky Mountain region prior to and during the Laramide orogeny," *Geological Society of America Bulletin*, vol. 128, nos. 5–6, pp. 973–988, 2016.

[91] E. D. Humphreys, "Post-Laramide removal of the Farallon slab, western United States," *Geology*, vol. 23, no. 11, 1995.

[92] P. Guth, D. Schmidt, J. Deibert, and J. Yount, "Tertiary extensional basins of northwestern Clark County, Nevada," in *This Extended Land—Geological Journeys in the Southern Basin and Range: Geological Society of America, Cordilleran Section, Field Trip Guidebook*, D.L. Weide, and M.L. Faber, Eds., pp. 239–254, Geological Society of America, 1988.

[93] R. H. Groshong, *3-D Structural Geology*, Springer, Berlin, Heidelberg, 2006.

[94] M. Evans and W. J. Taylor, Structural development and tectonic role of the Arrowhead Mine fault, Pahranagat shear zone, Nevadain *112th Annual GSA Cordilleran Section Meeting*, p. 30, American Association of Petroleum Geologists, Oxnard, CA, 2015.

[95] J.-E. Lundstern, C. M. Mercer, and L. E. Morgan, "U-Pb detrital zircon data and Ar feldspar data from middle Cenozoic sandstones and volcanic tuffs exposed in several parts of southern Nevada, USA," *U.S. Geological Survey Data Release*, 2023.

[96] K. F. Kuiper, A. L. Deino, F. J. Hilgen, W. Krijgsman, P. R. Renne, and J. R. Wijbrans, "Synchronizing rock clocks of Earth history," *Science*, vol. 320, no. 5875, pp. 500–504, 2008.

[97] G. B. Dalrymple, E. C. Alexander, M. A. Lanphere, and G. P. Kraker, "Irradiation of samples for 40Ar/39Ar dating using the Geological Survey TRIGA reactor," in *US Geological Survey Professional Paper 1176*. Vol. 55, 1981.

[98] I. McDougall and T. M. Harrison, "Geochronology and theromochronology by the 40Ar/39 Ar method," 2nd Ed, Oxford University Press, New York, NY, 1999.

[99] J. Ross, "NMGRL/Pychron V18.2," *Zenodo*, 2019.

[100] K. Min, R. Mundil, P. R. Renne, and K. R. Ludwig, "A test for systematic errors in 40Ar/39Ar geochronology through comparison with U/Pb analysis of a 1.1-Ga rhyolite," *Geochimica et Cosmochimica Acta*, vol. 64, no. 1, pp. 73–98, 2000.

[101] J. Taylor, *Introduction to Error Analysis: The Study of Uncertainties in Physical Measurements*. 2nd Edition, Published by University Science Books, Sausalito, California, 1997.

[102] I. Wendt and C. Carl, "The statistical distribution of the mean squared weighted deviation," *Chemical Geology: Isotope Geoscience Section*, vol. 86, no. 4, pp. 275–285, 2023.

[103] K. I. Mahon, "The New 'York' regression: application of an improved statistical method to geochemistry," *International Geology Review*, vol. 38, no. 4, pp. 293–303, 1996.

[104] R. Pearson, *Exploring Data in Engineering, the Sciences, and Medicine*, Oxford University Press, New York, NY, 2011.

[105] G. E. Gehrels, V. A. Valencia, and A. Pullen, "Detrital zircon geochronology by laser-ablation multicollector ICPMS at the Arizona Laserchron Center," *The Paleontological Society Papers*, vol. 12, pp. 67–76, 2006.

[106] G. E. Gehrels, V. A. Valencia, and J. Ruiz, "Enhanced precision, accuracy, efficiency, and spatial resolution of U-Pb ages by laser ablation-multicollector-inductively coupled plasma-mass spectrometry," *Geochemistry, Geophysics, Geosystems*, vol. 9, no. 3, pp. 1–13, 2008.

[107] J. B. Paces and J. D. Miller, "Precise U-Pb ages of Duluth complex and related mafic intrusions, northeastern Minnesota: Geochronological insights to physical, petrogenetic, paleomagnetic, and tectonomagmatic processes associated with the 1.1 Ga Midcontinent Rift system," *Journal of Geophysical Research*, vol. 98, no. B8, pp. 13997–14013, 1993.

[108] J. M. Mattinson, "Analysis of the relative decay constants of 235U and 238U by multi-step CA-TIMS measurements of closed-system natural zircon samples," *Chemical Geology*, vol. 275, nos. 3–4, pp. 186–198, 2010.

[109] L. Nasdala, W. Hofmeister, N. Norberg, et al., "Zircon M257 - A homogeneous natural reference material for the ion microprobe U-Pb analysis of zircon," *Geostandards and Geoanalytical Research*, vol. 32, no. 3, pp. 247–265, 2008.

[110] L. P. Black, S. L. Kamo, C. M. Allen, et al., "Improved 206Pb/238U microprobe geochronology by the monitoring of a trace-element-related matrix effect; SHRIMP, ID–TIMS, ELA–ICP–MS and oxygen isotope documentation for a series of zircon standards," *Chemical Geology*, vol. 205, nos. 1–2, pp. 115–140, 2004.

[111] K. E. Sundell, G. E. Gehrels, and M. E. Pecha, "Rapid U-Pb geochronology by laser ablation multi-collector ICP-MS," *Geostandards and Geoanalytical Research*, vol. 45, no. 1, pp. 37–57, 2021.

[112] G. R. Sharman, J. P. Sharman, and Z. Sylvester, "detritalPy: a python-based toolset for visualizing and analysing detrital geo-thermochronologic data," *The Depositional Record*, vol. 4, no. 2, pp. 202–215, 2018.

[113] W. R. Dickinson and G. E. Gehrels, "Use of U–Pb ages of detrital zircons to infer maximum depositional ages of strata: a test against a Colorado Plateau Mesozoic database," *Earth and Planetary Science Letters*, vol. 288, nos. 1–2, pp. 115–125, 2009.

[114] D. S. Coutts, W. A. Matthews, and S. M. Hubbard, "Assessment of widely used methods to derive depositional ages from detrital zircon populations," *Geoscience Frontiers*, vol. 10, no. 4, pp. 1421–1435, 2019.

[115] P. Copeland, "On the use of geochronology of detrital grains in determining the time of deposition of clastic sedimentary strata," *Basin Research*, vol. 32, no. 6, pp. 1532–1546, 2020.

[116] P. Vermeesch, "Maximum depositional age estimation revisited," *Geoscience Frontiers*, vol. 12, no. 2, pp. 843–850, 2021.

[117] L. P. Black, "Recent Pb loss in zircon: a natural or laboratory-induced phenomenon?," *Chemical Geology*, vol. 65, no. 1, pp. 25–33, 1987.

[118] A. von Quadt, D. Gallhofer, M. Guillong, I. Peytcheva, M. Waelle, and S. Sakata, "U–Pb dating of CA/non-CA treated zircons obtained by LA-ICP-MS and CA-TIMS techniques: Impact for their geological interpretation," *J. Anal. At. Spectrom.*, 2014.

[119] K. E. Watts, M. A. Coble, J. A. Vazquez, C. D. Henry, J. P. Colgan, and D. A. John, "Chemical abrasion-SIMS (CA-SIMS) U-Pb dating of zircon from the late Eocene Caetano Caldera, Nevada," *Chemical Geology*, vol. 439, pp. 139–151, 2016.

[120] T. M. Herriott, J. L. Crowley, M. D. Schmitz, M. A. Wartes, and R. J. Gillis, "Exploring the law of detrital zircon: LA-ICP-MS and CA-TIMS geochronology of Jurassic forearc strata, Cook Inlet, Alaska, USA," *Geology*, 2019.

[121] C. B. Keller, P. Boehnke, B. Schoene, and T. M. Harrison, "Stepwise chemical abrasion–isotope dilution–thermal ionization mass spectrometry with trace element analysis of microfractured Hadean zircon," *Physical Sciences and Mathematics*, vol. 1, no. 1, pp. 85–97, 2019.

[122] M. S. A. Horstwood, J. Košler, G. Gehrels, S. E. Jackson, N. M. McLean, C. Paton, et al., "Community-derived standards for LA-ICP-MS U-(Th-)Pb geochronology – uncertainty propagation, age interpretation and data reporting," *Geostandards and Geoanalytical Research*, 2016.

[123] M. G. Best, E. H. Christiansen, A. L. Deino, S. Gromme, G. L. Hart, and D. G. Tingey, "The 36–18 Ma Indian Peak-Caliente ignimbrite field and calderas, southeastern Great Basin, USA: Multicyclic super-eruptions," *Geosphere*, vol. 9, no. 4, pp. 864–950, 2013.

[124] M. A. Lamb, L. S. Beard, M. Dragos, et al., "Provenance and paleogeography of the 25–17 Ma Rainbow Gardens formation: evidence for tectonic activity at ca. 19 Ma and internal drainage rather than throughgoing paleorivers on the southwestern Colorado Plateau," *Geosphere*, vol. 14, no. 4, pp. 1592–1617, 2018.

[125] M. Lamb, L. S. Beard, T. Hickson, et al., "Late Oligocene–early Miocene landscape evolution of the Lake Mead region during the transition from Sevier contraction to Basin and

Range extension," *Geological Society of America Bulletin*, 2015.

[126] M. G. Best, S. Gromme, A. L. Deino, E. H. Christiansen, G. L. Hart, and D. G. Tingey, "The 36–18 Ma Central Nevada ignimbrite field and calderas, Great Basin, USA: multicyclic super-eruptions," *Geosphere*, vol. 9, no. 6, pp. 1562–1636, 2013.

[127] R. E. Anderson and L. F. Hintze, "Geologic map of the Dodge Spring quadrangle, Washington County, Utah, and Lincoln County, Nevada," *US Geological Survey Geologic Quadrangle Map GQ-1721*, 1993.

[128] P. D. Rowley, V. S. Williams, G. S. Vice, D. J. Maxwell, D. B. Hacker, L. W. Snee, et al., "Interim geologic map of the Cedar City 30' × 60' quadrangle, Iron and Washington Counties, Utah," Utah Geological Survey Open-File Report 476DM, 2006.

[129] S. B. Castor, "Geologic map of the Frenchman Mountain quadrangle, Clark County, Nevada," *Nevada Bureau of Mines and Geology Map*, 2000.

[130] D. W. Moore and A. W. Straub, "Correlation of Upper Cretaceous and Paleogene(?) rocks beneath the Claron formation, Crow Creek, western Markagunt Plateau, southwest Utah," in *The Geologic Transition, High Plateaus to Great Basin - A Symposium and Field Guide (The Mackin Volume)*, pp. 75–95, Utah Geological Association Publication 30 - Pacific Section American Association of Petroleum Geologists Publication GB78, 2001.

[131] L. A. Wright and B. W. Troxel, "Geologic map of the central and northern Funeral mountains and adjacent areas, Death Valley region, southern California," in *U.S. Geological Survey Miscellaneous Investigations Series Map I-2305*, 1993.

[132] E. Lander, "Early late Duchesnean (late middle Eocene) Titus Canyon fauna, Titus Canyon Formation, Death Valley National Park, Inyo County, southeastern California," in *Exploring Ends of Eras in the Eastern Mojave Desert, Desert Symposium Field Guide and Proceedings*, D.M. Miller, Ed., pp. 141–153, Desert Hot Springs, California, 2019.

[133] T. M. Schwartz and R. K. Schwartz, "Paleogene postcompressional intermontane basin evolution along the frontal Cordilleran fold-and-thrust belt of southwestern Montana," *Geological Society of America Bulletin*, vol. 125, nos. 5–6, pp. 961–984, 2013.

[134] A. D. Miall, "Lithofacies types and vertical profile models in braided river deposits: a summary," *Canadian Society of Petroleum Geologists Memoir 5*, 597–604, 1977.

[135] R. B. Scott, W. C. Swadley, and B. Byron, Preliminary geologic map of the Pahroc Spring quadrangle, Lincoln County, Nevada, *US Geological Survey Open-File Report 92-423*, 1992.

[136] W. J. Taylor, J. M. Bartley, D. R. Lux, and G. J. Axen, Timing of tertiary extension in the Railroad Valley-Pioche transect, Nevada: constraints from 40Ar/39Ar ages of volcanic rocks *Journal of Geophysical Research*, vol. 94, no. B6, pp. 7757–7774, 1989.

[137] R. B. Scott, W. C. Swadley, and W. J. Taylor, Preliminary geologic map of the Wheatgrass Spring quadrangle, Lincoln County, Nevada *US Geological Survey Open-File Report 94-175*, 1994.

[138] W. J. Taylor, "Chapter 8: Spatial and temporal relations of Cenozoic volcanism and extension in the North Pahroc and Seaman Ranges, eastern Nevada," in *Basin and Range Extensional Tectonics Near the Latitude of Las Vegas, Nevada*, B.P. Wernicke, Ed., Geological Society of America, 1990.

[139] P. D. Rowley, R. R. Shroba, F. W. Simonds, K. J. Burke, G. J. Axen, and S. D. Olmore, "Geologic map of the Chief Mountain quadrangle, Lincoln County, Nevada," *U.S. Geological Survey Open-File Report 91-135*, 1994.

[140] J. J. Anderson and P. D. Rowley, "Cenozoic stratigraphy of southwestern high plateaus of Utah," in *Geological Society of America Special Paper 160: Cenozoic Geology of Southwestern High Plateaus of Utah*, J.J. Anderson, P.D. Rowley, R.J. Fleck, and A.E.M. Narin, Eds., 1975.

[141] L. F. Hintze, "Stratigraphy and structure of the Beaver Dam Mountains, southwestern Utah," in *Thrusting and Extensional Structures and Mineralization in the Beaver Dam Mountains, Southwestern Utah*, Utah Geological Association, 1986.

[142] E. G. Sable and F. Maldonado, "The Brian Head Formation (revised) and selected Tertiary sedimentary rock units, Markagunt Plateau and adjacent areas, southwestern Utah," in *US Geological Survey Bulletin 2153-A: Geologic studies in the Basin and Range-Colorado Plateau transition in southeastern Nevada, southwestern Utah, and northwestern Arizona*, F. Maldonado, and L.D. Nealey, Eds., pp. 61–77, 1995.

[143] W. C. Swadley, W. R. Page, R. B. Scott, and E. H. Pampeyan, "Geologic map of the Delamar 3 SE quadrangle, Lincoln County, Nevada," *US Geological Survey Geologic Quadrangle Map 1754*, 1994.

[144] S. R. Haynes, "Development of the Eocene Elko Basin, northeastern Nevada: Implications for paleogeography and regional tectonism," The University of British Columbia [M.S. thesis], 2003.

[145] C. D. Henry, "Ash-flow tuffs and paleovalleys in northeastern Nevada: implications for Eocene paleogeography and extension in the Sevier hinterland, northern Great Basin,"*Geosphere*, vol. 4, no. 1, p. 1, 2008.

[146] M. W. Ressel and C. D. Henry, "Igneous geology of the Carlin trend, Nevada: development of the Eocene plutonic complex and significance for Carlin-type gold deposits," *Economic Geology*, vol. 101, no. 2, pp. 347–383, 2006.

[147] R. F. Dubiel, C. J. Potter, S. C. Good, and L. W. Snee, "Reconstructing an Eocene extensional basin: The White Sage Formation, eastern Great Basin," in *Reconstructing the History of Basin and Range Extension Using Sedimentology and Stratigraphy: Geological Society of America Special Paper 303*, K.K. Beratan, Ed., pp. 1–14, Geological Society of America, 1996.

[148] A. Ruksznis, Geology and Geochronology of Cenozoic Sedimentary Basins, East-Central Nevada Stanford University [M.S. thesis], Stanford, CA, 2015.

[149] R. E. Anderson, T. P. Barnhard, and L. W. Snee, "Roles of plutonism, midcrustal flow, tectonic rafting, and horizontal collapse in shaping the Miocene strain field of the Lake Mead area, Nevada and Arizona," *Tectonics*, vol. 13, no. 6, pp. 1381–1410, 1994.

[150] C. R. Longwell, "Measure and date of movement on Las Vegas Valley shear zone, Clark County, Nevada," *Geological Society of America Bulletin*, vol. 85, no. 6, 1974.

[151] R. G. Bohannon, J. A. Grow, J. J. Miller, and R. H. Blank, Jr., "Seismic stratigraphy and tectonic

development of Virgin River depression and associated basins, southeastern Nevada and northwestern Arizona," *Geological Society of America Bulletin*, vol. 105, no. 4, pp. 501–520, 1993.

[152] T. A. Hickson, A. J. Ness, and M. A. Lamb, "Miocene tectonics and climate in the Lake Mead region recorded by Horse Spring formation carbonates," in *Geological Society of America Special Paper 463*, P.J. Umhoefer, L.S. Beard, and M.A. Lamb, Eds., pp. 121–145, 2010.

[153] M. A. Lamb, K. L. Martin, T. A. Hickson, P. J. Umhoefer, and L. Eaton, "Stratigraphy and age of the lower Horse Spring formation in the Longwell Ridges area, southern Nevada: Implications for tectonic interpretations," in *Geological Society of America Special Paper 463*, P.J. Umhoefer, L.S. Beard, and M.A. Lamb, Eds., pp. 171–201, 2010.

[154] L. Liu and M. Gurnis, "Dynamic subsidence and uplift of the Colorado Plateau," *Geology*, vol. 38, no. 7, pp. 663–666, 2010.

[155] E. D. Humphreys, "Relation of flat subduction to magmatism and deformation in the western United States," in *Geological Society of America Memoir 204: Backbone of the Americas: Shallow Subduction, Plateau Uplift, and Ridge and Terrane Collision*, S.M. Kay, V.A. Ramos, and W.R. Dickinson, Eds., pp. 85–98, 2009.

[156] W. R. Dickinson, "Cenozoic plate tectonic setting of the Cordilleran region in the United States," in *Cenozoic Paleogeography of the Western United States*, J.M. Armentrout, M.R. Cole, and T. H, Eds., pp. 1–13, Pacific Section, Society of Economic Paleontologists and Mineralogists, Los Angeles, California, 1979.

[157] W. P. Schellart, D. R. Stegman, R. J. Farrington, J. Freeman, and L. Moresi, "Cenozoic tectonics of western North America controlled by evolving width of Farallon slab," *Science*, vol. 329, no. 5989, pp. 316–319, 2010.

[158] J. Zachos, M. Pagani, L. Sloan, E. Thomas, and K. Billups, "Trends, rhythms, and aberrations in global climate 65 Ma to present," *Science*, vol. 292, no. 5517, pp. 686–693, 2001.

[159] T. M. Schwartz, K. Methner, A. Mulch, S. A. Graham, and C. P. Chamberlain, "Paleogene topographic and climatic evolution of the northern Rocky Mountains from integrated sedimentary and isotopic data," *GSA Bulletin*, vol. 131, nos. 7–8, pp. 1203–1223, 2019.

[160] D. S. Vandervoort and J. G. Schmitt, "Cretaceous to early tertiary paleogeography in the hinterland of the Sevier thrust belt, east-central Nevada," *Geology*, vol. 18, no. 6, pp. 567–570, 1990.

[161] E. J. Cassel, M. E. Smith, and B. R. Jicha, "The impact of slab rollback on Earth's surface: Uplift and extension in the hinterland of the North American Cordillera," *Geophysical Research Letters*, vol. 45, no. 20, pp. 10996–11004, 2018.

[162] J. P. Colgan, K. A. Howard, R. J. Fleck, and J. L. Wooden, "Rapid middle Miocene extension and unroofing of the southern Ruby Mountains, Nevada," *Tectonics*, vol. 29, no. 6, 2010.

[163] R. E. Anderson, M. L. Zoback, and G. A. Thompson, "Implications of selected subsurface data on the structural form and evolution of some basins in the northern Basin and Range Province, Nevada and Utah (USA)," *Geological Society of America Bulletin*, vol. 94, no. 9, pp. 1055–1072, 1983.

[164] J. H. Stewart, "1: Basin-range structure in western North America: A review," in *Geological Society of America Memoir 152: Cenozoic Tectonics and Regional Geophysics of the Western Cordillera*, R.B. Smith, and G.P. Eaton, Eds., pp. 1–31, 1978.

[165] S. M. Bohaty, J. C. Zachos, F. Florindo, and M. L. Delaney, "Coupled greenhouse warming and deep-sea acidification in the middle Eocene," *Paleoceanography*, vol. 24, no. 2, 2009.

[166] C. M. John, S. M. Bohaty, J. C. Zachos, et al., "North American continental margin records of the Paleocene-Eocene thermal maximum: Implications for global carbon and hydrological cycling," *Paleoceanography*, vol. 23, no. 2, pp. 1–20, 2008.

[167] M. E. Smith, E. J. Cassel, B. R. Jicha, B. S. Singer, and A. S. Canada, "Hinterland drainage closure and lake formation in response to middle Eocene Farallon slab removal, Nevada, U.S.A.," Earth and Planetary Science Letters, vol. 479, pp. 156–169, 2017.

[168] M. G. Best and E. H. Christiansen, "Limited extension during peak tertiary volcanism, Great Basin of Nevada and Utah," *Journal of Geophysical Research*, vol. 96, no. B8, pp. 13509–13528, 1991.

[169] K. L. Pierce and L. A. Morgan, "Chapter 1: The track of the Yellowstone hot spot: Volcanism, faulting, and uplift," in *Regional Geology of Eastern Idaho and Western Wyoming*, P.K. Link, M.A. Kuntz, and L.B. Piatt, Eds., Geological Society of America, 1992.

[170] J. P. Colgan and C. D. Henry, "Eruptive history, geochronology, and post-eruption structural evolution of the late Eocene Hall Creek caldera, Toiyabe Range, Nevada," *U.S. Geological Survey Professional Paper 1832*, 2017.

[171] W. R. Dickinson, "Geotectonic evolution of the Great Basin," *Geosphere*, vol. 2, no. 7, pp. 353–368, 2006.

[172] N. J. Van Buer and E. L. Miller, "Sahwave batholith, NW Nevada: Cretaceous arc flare-up in a basinal terrane," *Lithosphere*, vol. 2, no. 6, pp. 423–446, 2010.

[173] S A. Reid, "Late Cretaceous and Paleogene sedimentation along east side of San Joaquin Basin, California," in *Studies of the Geology of the San Joaquin Valley*, S. A. Graham, Ed., pp. 157–171, Society for Sedimentary Geology, Pacific Section, SEPM, 1988.

[174] M. D. Evans, "Structural evolution and regional implications of the Arrowhead Mine fault within the Pahranagat shear zone," University of Nevada Las Vegas, Las Vegas, Nevada [Masters thesis], 2018.

[175] L. J. Sonder and C. H. Jones, "Western United States extension: how the west was widened," *Annual Review of Earth and Planetary Sciences*, vol. 27, no. 1, pp. 417–462, 1999.

[176] W. R. Dickinson, "Phanerozoic palinspastic reconstructions of Great Basin geotectonics (Nevada-Utah, USA)," *Geosphere*, vol. 9, no. 5, pp. 1384–1396, 2013.

[177] J. B. Chapman, S. E. Runyon, J. E. Shields, et al., "The North American Cordilleran anatectic belt," *Earth-Science Reviews*, vol. 215, no. 103576, 2021.

[178] L. S. Beard, R. E. Anderson, D. L. Block, R. G. Bohannon, R. J. Brady, S. B. Castor, et al., "Preliminary geologic map of the Lake Mead 30' X 60' quadrangle, Clark County, Nevada, and Mohave County, Arizona," US Geological Survey Open-File Report 2007-1010, 2007.

[179] J. H. Stewart and J. E. Carlson, "Geologic map of Nevada," *U.S. Geological Survey Unnumbered Series*, 1978.

[180] B. P. Wernicke, G. J. Axen, and J. K. Snow, "Basin and range extensional tectonics at the latitude of Las Vegas, Nevada," *Geological Society of America Bulletin*, vol. 100, no. 11, pp. 1738–1757, 1988.

[181] W. R. Page, S. C. Lundstrom, A. G. Harris, V. E. Langenheim, J. B. Workman, S. A. Mahan, et al., "Geologic and geophysical maps of the Las Vegas 30′ × 60′ quadrangle, Clark and Nye counties, Nevada, and Inyo County, California," *US Geological Survey Scientific Investigations Map 2814*, 2005.

[182] T. J. Felger and L. S. Beard, "Geologic map of Lake Mead and surrounding regions, southern Nevada, southwestern Utah, and northwestern Arizona," in *Geological Society of America Special Paper 463*, P.J. Umhoefer, L.S. Beard, and M.A. Lamb, Eds., 2010.

[183] D. A. Sawyer, R. J. Fleck, M. A. Lanphere, R. G. Warren, D. E. Broxton, and M. R. Hudson, "Episodic caldera volcanism in the Miocene southwestern Nevada volcanic field: Revised stratigraphic framework, 40Ar/39Ar geochronology, and implications for magmatism and extension," *Geological Society of America Bulletin*, vol. 106, no. 10, pp. 1304–1318, 1994.

[184] P. D. Rowley, L. D. Nealey, D. M. Unruh, L. W. Snee, H. H. Mehnert, R. E. Anderson, et al., "Stratigraphy of Miocene ash-flow tuffs in and near the Caliente caldera complex, southeastern Nevada and southwestern Utah," in *U.S. Geological Survey Bulletin 2056-B: Geologic Studies in the Basin and Range-Colorado Plateau Transition in Southeastern Nevada, Southwestern Utah, and Northwestern Arizona*, R.B. Scott, and W.C. Swadley, Eds., pp. 47–88, U.S. Geological Survey, Washington, D.C, 1992.

[185] L. D. Nealey, P. D. Rowley, D. M. Unruh, J. R. Budahn, L. W. Snee, and H. H. Mehnert, "Preliminary geochemistry of Miocene ash-flow Tuffs in and near the Caliente Caldera complex, southeastern Nevada and Southwestern Utah," in *U.S. Geological Survey Bulletin 2056-B: Geologic Studies in the Basin and Range-Colorado Plateau Transition in Southeastern Nevada, Southwestern Utah, and Northwestern Arizona*, R.B. Scott, and W.C. Swadley, Eds., pp. 91–110, U.S. Geological Survey, Washington, D.C, 1992.